In Cooperation with the Southern Nevada Water Authority

Audiomagnetotelluric Data and Two-Dimensional Models from Spring, Snake, and Three Lakes Valleys, Nevada

By Darcy K. McPhee, Bruce A. Chuchel, and Louise Pellerin

Report Series 2007–1181

U.S. Department of the Interior
U.S. Geological Survey

U.S. Department of the Interior
DIRK KEMPTHORNE, Secretary

U.S. Geological Survey
Mark D. Myers, Director

U.S. Geological Survey, Reston, Virginia 2007

For product and ordering information:
World Wide Web: http://www.usgs.gov/pubprod
Telephone: 1-888-ASK-USGS

For more information on the USGS—the Federal source for science about the Earth, its natural and living resources, natural hazards, and the environment:
World Wide Web: http://www.usgs.gov
Telephone: 1-888-ASK-USGS

Suggested citation:
McPhee, Darcy K., Chuchel, Bruce A., and Pellerin, Louise, 2007, Audiomagnetotelluric data and two-dimensional models from Spring, Snake, and Three Lakes Valleys, Nevada: U.S. Geological Survey Open-File Report 2007-1181, 47 p. [http://pubs.usgs.gov/of/2007/1181/].

Any use of trade, product, or firm names is for descriptive purposes only and does not imply endorsement by the U.S. Government.

Although this report is in the public domain, permission must be secured from the individual copyright owners to reproduce any copyrighted material contained within this report.

Contents

Abstract 5
Introduction 5
Audiomagnetotelluric Method 7
Audiomagnetotelluric Data 8
2-D Inverse Modeling 9
AMT Surveys and Results 10
  Spring Valley 10
    Profiles SVNF, SVNH, SVNI- Schell Creek Range 10
    Profile SVNG- Fortification Range 11
    Profiles SVNM, SVNK, SVNL, SVNJ- Southern Snake Range 11
  Snake Valley 12
    Profiles SNKA, SNKB, SNKC 12
  Three Lakes Valley 13
    Profiles TLVA, TLVC 13
Acknowledgments 14
References Cited 14

Figures

Figure 1. Topographic map of study area showing location of AMT profiles in Spring and Snake Valleys. Profiles A and B were collected in 2004 and are presented in McPhee and others (2006). 17
Figure 2. Topographic map of study area showing location of AMT profiles in southern Three Lakes Valley. 18
Figure 3. 2-D inverse model computed from the TM mode data along profile SVNF in Spring Valley. 19
Figure 4. Pseudosections of observed data and model response for the apparent resistivity and phase along profile SVNF. Black dots show data points. 20
Figure 5. 2-D inverse model computed from the TM mode data along profile SVNH in Spring Valley. 21
Figure 6. Pseudosections of observed data and model response for the apparent resistivity and phase along profile SVNH. Black dots show data points. 22
Figure 7. 2-D inverse model computed from the TM mode data along profile SVNI in Spring Valley. 23
Figure 8. Pseudosections of observed data and model response for the apparent resistivity and phase along profile SVNI. Black dots show data points. 24
Figure 9. 2-D inverse model computed from the TM mode data along profile SVNG in Spring Valley. 25
Figure 10. Pseudosections of observed data and model response for the apparent resistivity and phase along profile SVNG. Black dots show data points. 26
Figure 11. 2-D inverse model computed from the TM mode data along profile SVNM in Spring Valley. 27

Figure 12. Pseudosections of observed data and model response for the apparent resistivity and phase along profile SVNM. Black dots show data points. 28
Figure 13. 2-D inverse model computed from the TM mode data along profile SVNK in Spring Valley. 29
Figure 14. Pseudosections of observed data and model response for the apparent resistivity and phase along profile SVNK. Black dots show data points. 30
Figure 15. 2-D inverse model computed from the TM mode data along profile SVNL in Spring Valley. 31
Figure 16. Pseudosections of observed data and model response for the apparent resistivity and phase along profile SVNL. Black dots show data points. 32
Figure 17. Pseudosections of observed data only for the TE and TM mode apparent resistivity and phase along profile SVNJ. 33
Figure 18. 2-D inverse model computed from the TM mode data along profile SNKA in Snake Valley. Note that resistivity scale is different from that used in Spring Valley models. 34
Figure 19. Pseudosections of observed data and model response for the apparent resistivity and phase along profile SNKA. Black dots show data points. 35
Figure 20. 2-D inverse model computed from the TM mode data along profile SNKB in Snake Valley. 36
Figure 21. Pseudosections of observed data and model response for the apparent resistivity and phase along profile SNKB. Black dots show data points. 37
Figure 22. 2-D inverse model computed from the TM mode data along profile SNKC in Snake Valley. 38
Figure 23. Pseudosections of observed data and model response for the apparent resistivity and phase along profile SNKC. Black dots show data points. 39
Figure 24. 2-D inverse model computed from the TE+TM mode data along profile TLVA in Three Lakes Valley. Note that resistivity scale is different from that used in Spring and Snake Valley models. 40
Figure 25. Pseudosections of observed data and model response for the apparent resistivity and phase along profile TLVA for both the TE (a) and TM (b) modes. Black dots show data points. 40
Figure 26. 2-D inverse model computed from the TE+TM mode data along profile TLVC in Three Lakes Valley. 41
Figure 27. Pseudosections of observed data and model response for the apparent resistivity and phase along profile TLVC for both the TE (a) and TM (b) modes. Black dots show data points. 41

Tables

Table 1. Description of AMT profiles. 42
Table 2. Sounding numbers, locations, elevations and azimuths of stations along AMT profiles. 43

Appendix

A. Sounding curves. 47

Audiomagnetotelluric data and two-dimensional models from Spring, Snake, and Three Lakes Valleys, Nevada

By Darcy K. McPhee[1], Bruce A. Chuchel[1], and Louise Pellerin[2]

Abstract

Audiomagnetotelluric (AMT) data along thirteen profiles in Spring, Snake, and Three Lakes Valleys, and the corresponding two-dimensional (2-D) inverse models, are presented. The AMT method is a valuable tool for estimating the electrical resistivity of the Earth over depth ranges of a few meters to roughly one kilometer. It is important for revealing subsurface structure and stratigraphy within the Basin and Range province of eastern Nevada that can be used to define the geohydrologic framework of the region. We collected AMT data using the Geometrics StrataGem EH4 system. Profiles were 1.2 to 4.6 km in length with station spacing of 100-400 m. Data were recorded in a coordinate system parallel to and perpendicular to the assumed regional geologic strike direction. We show station locations, sounding curves of apparent resistivity, phase, and coherency, and 2-D models. The 2-D inverse models are computed from the transverse electric (TE), transverse magnetic (TM), and TE+TM mode data using the conjugate gradient, finite-difference method of Rodi and Mackie (2001). Preliminary interpretation of these models defines the structural framework of the basins and the resistivity contrasts between alluvial basin-fill, volcanic units, and carbonate/clastic rocks.

Introduction

The Basin and Range province is an arid, mountainous, sparsely populated region of the western United States. Ground-water is organized into extensive regional systems (Harrill and Prudic, 1998) where it can flow between adjacent topographic ranges and basins. The location of basin-fill aquifers, including carbonate rocks, and their hydraulic connectivity to the carbonate-rock aquifer system that underlies the entire eastern two-thirds of the Great Basin (Plume, 1996; Harrill and Prudic, 1998) is important for assessing ground-water resources in the region. Range-front

[1] U.S. Geological Survey, 345 Middlefield Rd., MS 989, Menlo Park, CA 94025
[2] Green Engineering, Inc., 2215 Curtis St., Berkeley, CA 94702

faults are a primary structural control on the hydrogeology of the valleys in eastern Nevada, however, structure within the basins is often obscured by basin-fill sediments, hence geophysical investigations are needed to characterize the subsurface structures and stratigraphy influencing ground-water resources. The gravity method has been used to estimate the structure and depth of the basins in eastern Nevada (Mankinen and others, 2007; Mankinen and others, 2006; Scheirer, 2005), but because densities of volcanic rocks in the area may be comparable to the average density of basin sediment-fill, comprised of semi-consolidated to unconsolidated sand, gravel, silt, clay, and local evaporites, it may be difficult to resolve the subsurface geometry of the basin-fill and volcanic rocks using the gravity method alone.

Previous results from eastern Nevada (McPhee and others, 2006), including studies in Spring Valley, show that two-dimensional (2-D) inversion of audiomagnetotelluric (AMT) sounding data defines significant structure within the upper kilometer of the subsurface in a typical basin setting. Detailed structure was observed within alluvial basins such as clear transitions between unsaturated and saturated alluvium/volcanic rocks, high-resistivity (>1000 ohm-m) carbonate rocks, and the locations of range-front and intra-basin faults. In some cases AMT models defined the shape of and depth to the basement, which correlated well with depth to basement estimates derived from inversion of gravity data (Mankinen and others, 2006).

In this study, the AMT method is used in Spring, Snake, and Three Lakes valleys (Figures 1 and 2) to define potential geologic/tectonic structures significant to ground-water exploration. Two separate field surveys were conducted in Spring Valley during Spring/Summer of 2006 using methods identical to those described in McPhee and others (2006). A survey in Snake Valley was conducted in the Fall of 2006, followed by another survey in Three Lakes Valley in April 2007. We were able to delineate range-front faults, structure, and stratigraphy within the basins as well as the overall framework of the basins. These models are being used to help site ground-water exploration wells and are contributing to the geologic framework for hydrologic modeling in the region.

The purpose of this report is to release the AMT sounding data and 2-D inverse models. Hydrogeologic interpretation of the models is not the focus of this report.

Audiomagnetotelluric Method

The magnetotelluric (MT) method is a geophysical technique that uses the Earth's natural electromagnetic (EM) fields as a source to investigate the electrical resistivity structure of the subsurface (Telford and others, 1991; Vozoff, 1991). Within the upper crust, the resistivity of geologic units is largely dependent upon their fluid content, porosity, degree of fracturing, temperature, and conductive mineral content (Keller, 1989). Saline fluids within pore spaces and fracture openings can reduce bulk resistivities by several orders of magnitude relative to the dry rock matrix. Resistivity can also be lowered by the presence of conductive clay minerals, graphite, and metallic sulfide mineralization. Up to temperatures of ~ 300 ºC, increased temperatures cause higher ionic mobility and mineral activation energy, reducing rock resistivities significantly (Nesbitt, 1993). Unaltered, unfractured igneous rocks are normally very resistive, with values typically 1,000 ohm-m or greater. Fault zones can appear as low resistivity units of less than 100 ohm-m when they are comprised of rocks fractured enough to host fluid transport and consequent mineralogical alteration (Eberhart-Phillips and others, 1995). Carbonate/clastic rocks are moderately to highly resistive, with values of hundreds to thousands of ohm-m depending upon their fluid content, porosity, fracturing, and impurities. Marine shale, mudstone, and clay-rich alluvium are normally very conductive with values of a few to tens of ohm-m. Unaltered, metamorphic, non-graphitic rocks are moderately to highly resistive. Tables of electrical resistivity for a variety of rocks, minerals and geological environments may be found in Keller (1987) and Palacky (1987).

Using the same theory, the AMT method is used to estimate the electrical resistivity of the Earth over depth ranges of a few meters to about one kilometer, employing a higher frequency range (Zonge and Hughes, 1991). The electrical impedance is a tensor quantity defined by the ratio of time-varying electric (E) to magnetic (H) field measured at the Earth’s surface. The surface impedance is a complex function of frequency; higher-frequency data are used for investigation of the near surface and lower-frequency data for greater depths. For a 2-D Earth, the diagonal terms of the impedance tensor are zero, and the off-diagonal terms can be decoupled into transverse electric (TE) and transverse magnetic (TM) modes. When the geology satisfies the 2-D assumption, the data for the TE mode measures electric field parallel to geologic strike, and that for the TM mode measures electric field perpendicular to geologic strike. This 2-D assumption permits significant simplification in the modeling and inversion of MT and AMT data. An AMT sounding

provides an estimate of resistivity beneath the receiver site and also indicates the geoelectric complexity at the sounding site. In areas where the resistivity distribution does not change rapidly from station to station, the resistivity sounding provides a reasonable estimate of the resistivity layering beneath the site.

The Geometrics StrataGem EH-4 system utilizes both natural and controlled-source electromagnetic signals to obtain a continuous electrical sounding of the Earth beneath the measurement site (Geometrics, 2000). Data are recorded from 92,000 to 10 Hz. The natural field strength is weak around 1,000 Hz so the controlled source is used to augment the natural field. Surface impedance results are immediately displayed as a resistivity sounding. Data are subsequently modeled using a 2-D inversion algorithm (see 2-D Inverse Modeling section). A more thorough discussion of the Stratagem EH-4 system used in this study is contained in Geometrics (2000) and McPhee and others (2006).

Audiomagnetotelluric Data

After transforming the recorded time-series data to the frequency domain, EM transfer functions are estimated (Geometrics, 2000) from which the apparent resistivity and phase tensor can be calculated at each site. Apparent resistivity is impedance magnitude normalized by frequency and the magnetic susceptibility for free space. The apparent resistivity and phase are related through a Hilbert transform; the phase is proportional to the slope of the apparent resistivity curve on a log-log plot, relative to a baseline of 45 degrees (Vozoff, 1991).

Predicted values of the electric field can be computed from the measured values of the magnetic field (Vozoff, 1991). The coherence of the predicted electric field with the measured electric field is a measure of the signal-to-noise ratio, which is displayed as a function of frequency in the E-predicted coherency plots. Coherency values lie between 0 and 1, where values at 0.5 denote signal levels equal to noise levels.

Several soundings were recorded at each station. The best sounding from each station is presented (Appendix A) and used in subsequent modeling of the data. The unedited data presented here are not rotated to the local geologic strike, but are fixed at specific azimuths as acquired in the field (Table 2). The ExHy mode is the nominal TM, and the EyHx the TE mode. Tensor data are calculated in the Imagem software (Geometrics, 2000). For each station, three separate panels are displayed in Appendix A: (1) Apparent resistivity, (2) Impedance phase, and (3) Coherency.

Electronic data are available upon request in two formats: Geometrics Z Impedance files (Geometrics, 2000; Appendix A) and the Electronic Data Interchange (EDI), which was established in 1987 by the Society of Exploration Geophysicists (SEG) as a standard format for the interchange of MT data (Wright, 1988).

2-D Inverse Modeling

Before modeling, impedance tensor data along each profile were rotated such that the E and H fields were approximately parallel and perpendicular to the regional geologic strike in the area. Based on the trends of faulting and geologic structures in these valleys, as well as depth to basement maps derived from gravity data, we chose our profiles in most cases to run roughly perpendicular to the geologic strike. Based on the 2-D nature of the geologic structures in all three valleys, we were fairly certain that we were working in 2-D environments. However, in some cases 3-D effects in the data were likely. Once mathematically rotated, spurious data and data with coherencies less than 0.75 were removed.

Dimensionality of each profile was determined by inspection of the data and dimensional analysis was performed if 3-D effects were suspect (Marti et al., 2005). Even in the presence of 3-D effects, 2-D modeling of the TM mode has been shown to be a robust approach (Wannamaker and others, 1984). We compute 2-D inverse models from the TE, TM, and TE+TM mode data using the conjugate gradient, finite-difference inversion of Rodi and Mackie (2001) for a range of starting models with many variations of regularization and smoothing parameters (Geosystem, 2005). We ran inversions both with and without topography, and we determined that the topography, which was fairly modest along each profile, did not affect the model results. Our preferred starting model along each profile used a 100 ohm-m half-space that included the topography. Other starting models were used to test model sensitivity and the depth of investigation. The primary criteria for choosing final models included the goodness of fit of the model response to the data as reported by the root mean square (RMS), the lack of artifacts in the model not supported by the data, and geological reasonableness of the model. RMS is commonly used to express the misfit between data and the model response. Misfits are normalized by the data error or the applied error floor. Misfits less than 1 fit the data to within the error bounds used in the inversion.

The AMT data on each profile are also displayed in pseudosection format with distance on the horizontal axis and period, the inverse of frequency, on the vertical axis (for example, see

Figure 4). As frequency is a non-linear proxy for depth, pseudosections represent qualitatively the variation of apparent resistivity and phase with depth. The calculated apparent resistivity and phase from the inverse model response is displayed for comparison and is used to judge the goodness of fit. Our preferred models represent the most robust results along each line using the cleanest data. Although the depth of exploration varies as a function of resistivity and frequency, we are showing a constant depth of investigation throughout each section.

AMT Surveys and Results

This section discusses details of each AMT survey as well as the 2-D models along each line. Two separate surveys were conducted in Spring Valley. In May 2006 we collected a total of four profiles (SVNF, SVNH, SVNI, SVNG) along the western margin of the valley (labeled F, H, I, G respectively, in Figure 1). In June 2006, we collected four more profiles (SVNM, SVNK, SVNL, SVNJ) along the eastern margin of southern Spring Valley (labeled M, K, L, J on Figure 1). In October 2006, we collected three profiles in Snake Valley (SNKA, SNKB, SNKC, Figure 1). Finally, in April 2007, we moved further south and collected two profiles in Three Lakes Valley (TLVA, TLVC, Figure 2). A description of each AMT profile is provided in Table 1, and individual sounding location information is contained in Table 2.

Overall, the AMT 2-D models define range-front and inter-basin faults, basin-fill alluvium, volcanic rocks, and carbonate/clastic rocks.

Spring Valley

Profiles SVNF, SVNH, SVNI- Schell Creek Range

Profiles F, H, and I were located in the western-central region of the valley and extended from the Schell Creek Range into the valley (Figure 1). Power transmission lines run east-west across Spring Valley several kilometers to the north of Profile H. Anthropomorphic noise, such as power lines, power generators, moving vehicles and trains, produce noise mainly affecting frequencies above 1 Hz, including the AMT observation frequency band. Data along each profile were noisy, despite the observation that the only known source of noise was the power lines several kilometers away.

The TE mode data were consistently noisier than those of the TM mode. Analysis of the rotational invariant parameters of the impedance tensor proposed by Weaver and others (2000) was

used to establish a classification of dimensionality associated with the measured data taking into account data errors (Marti and others, 2005; Ester Falgás Parra, personal communication). The data were determined to be quasi-1D in character, where structure varies slowly from that of a layered Earth. A 2-D Earth assumes that there is no variation within the strike direction. Faulted structures can be strongly 2-D or quasi-1D depending on the offset. In either case, a 2-D inversion strategy is justified. We show the preferred 2-D inverse models for Profiles F, H, and I (Figures 3-8) computed from the TM mode data. For the most part, equivalent models resulted when using the TE + TM mode, with a slightly higher RMS fit.

In western-central Spring Valley, the range front fault on the eastern side of the Schell Creek Range is well defined on all three profiles (Figures 3, 5, 7) and separates more resistive basement to the west from basin fill to the east. The models appear to define the shape of the valley and several inter-basin faults represented by resistivity contrasts can be delineated throughout the sections. We observe more conductive basin fill sediments along Profile H (Figure 5) than we do along profile F to the north and profile I to the south.

Profile SVNG- Fortification Range

Profile G was located in southwestern Spring Valley and extended from the Fortification Range east into the valley (Figure 1). Data along this profile were fairly noisy. According to the same dimensionality analysis and reasoning that was applied to Profiles F, H, and I, we can justify 2-D modeling here and computed our preferred 2-D model from the TM mode data using a 100 ohm-m starting space with topography (Figures 9,10).

The resistivity structure along Profile G shows the opposite trend in resistivity toward the east than was observed along Profiles F, H, and I. Here we observe a more conductive structure on the west juxtaposed by more resistive ‘basin fill’ to the east. Profile G originates very close to outcrops of tuff breccia, so the west end of the profile is likely located in the volcanic source region of the Fortification Range. The model likely shows a range front fault between fractured volcanic rocks to the west, likely part of the Indian Peak Caldera Complex (Best and others, 1989), and more consolidated and, therefore, resistive volcanic rocks to the east into the valley.

Profiles SVNM, SVNK, SVNL, SVNJ- Southern Snake Range

We collected four additional AMT profiles near the margin of the southern Snake Range in southeastern Spring Valley. Three of these profiles (SVNM, SVNK, SVNL) originated in the

Snake Range and extended west into the valley (Figure 1). There were no obvious sources of noise along these profiles. Profiles K, L, and M are oriented roughly perpendicular to the north-south geologic trend of the valley and the Snake Range, and we rotated the data along each profile such that the EM fields are oriented parallel and perpendicular to the range-front. We computed our preferred 2-D inverse models along each of these profiles from the TM mode data using a 100 ohm-m starting model with topography (Figures 11-16).

Profile M originated furthest east into the Snake Range, and the resulting model clearly shows a resistivity contrast likely in the location of a range-front fault separating resistive carbonate rocks of the Snake Range to the east with more conductive alluvial fill to the west (Figure 11). This contrast is less pronounced on Profile K (Figure 13) where the profile does not extend as far eastward into the range, however, a resistivity contrast at the east end of the line at an elevation of ~1400 m likely reflects the valley floor at this eastern margin. Profile L (Figure 15) maps two distinct carbonate bodies in the upper few hundred meters of the surface. These resistive structures (~ 500 ohm-m) are very similar to carbonate bodies observed along Profile A (Figure 1), ~1 km to the north (McPhee and others, 2006).

The fourth profile (SVNJ) extended roughly north-south across a pass between the southern Snake Range and the Limestone Hills (Figure 1). Profile J is unique in that it trends oblique to the assumed regional geologic. Further work is planned in this pass region between Spring Valley and Hamlin Valley; modeling will be based upon both past and future data. Data acquired to date is shown in pseudosection format (Figure 17).

Snake Valley

Profiles SNKA, SNKB, SNKC

Three AMT profiles (SNKA, SNKB, SNKC) were collected near the western margin of southern Snake Valley (Figure 1). These profiles extended into the range in the west and eastward into Snake Valley. A small north-south power line ran across the middle of SNKA (at a distance ~2400 m in Figure 18). This power line continued south and cut across SNKB at a distance ~3600 m (Figure 20) and was several kilometers away from the eastern end of SNKC. The power line was not a problem for stations at a distance greater than 200 m. The data in the high-frequency band (800-92,000 Hz), however, were noisy on all three profiles. After we completed the survey, we discovered that the transmitter that we were using to augment the natural source in the high-

frequency band was not operating correctly; only one of the two magnetic dipoles was transmitting. Consequently, we had to omit all of our high-frequency data. We computed 2-D models along each of these profiles using only the low-frequency data (10 Hz to ~ 800 Hz) and present only preliminary models here (Figures 18-23) computed from TM mode data. Consequently, values in the pseudosections from 100,000 to 1000 Hz, and in the model from the surface to ~150 m, are artifacts of contouring. Because only the low-frequency data were used, the models are very smooth being more robust and with lower RMS misfits than models computed from TE+TM mode data or with more restrictive regularization parameters. Models along all three profiles used a starting half-space model of 100 ohm-m with topography.

The extremely smooth models of SNKA and SNKB (Figures 18 and 20) show deep resistive features likely associated with crystalline rocks of the Snake Range while SNKC shows distinctly different, more conductive structure at depth.

Three Lakes Valley

Profiles TLVA, TLVC

We collected our final two AMT profiles (TLVA, TLVC) in southwestern Three Lakes Valley, roughly 300 km south of Spring Valley and about 35 km northwest of Las Vegas (Figure 2). Both profiles ended approximately 100-200 m north of a major highway (Hwy 95). A power line ran parallel to the highway on the south side, about 200-400 m from the ends of our profiles. There were no other sources of noise, and we collected clean data along the entire length of the profiles. TLVA and TLVC originated near fractured carbonate outcrops and extended roughly southwest into the valley. These profiles ran roughly perpendicular to the known NW-SE trending faults in the region but were oblique to the topography (Figure 2). The Las Vegas Valley Shear Zone (Langenheim and others, 1998) is a major structural feature in the region, and it cuts NW-SE though this part of the valley. Our objective was to image this shear zone and other faults in the area.

Through inspection of both modes, data show structure to be smoothly varying (quasi-1D) in the valley and crossing a structural contact in the middle of both profile lines consistent with the 2-D assumption. As seen in the data and resulting models, structural variations are predominant on the northern end of line where the profile lines separate; line TLVA shows quasi-1D responses while a distinct 2-D response is apparent on line TLVC. Our preferred 2-D models resulted from

TE+TM mode data using a 100 ohm-m starting model with topography (Figures 24-27). We ran several inversions using both the TM only and TE+TM mode data and found that the models resulting from the TE+TM mode data were more robust to varying parameters.

Models along TLVA and TLVC were consistent with each other as well as the local, outcropping geology. Both models image resistive (> 1000 ohm-m) carbonate structures at the northeastern end of the profiles. In addition, the shear zone can be seen cutting through the center of both profiles (at ~ 1000 m along TLVA and ~ 900 m along TLVC) juxtaposing more resistive carbonate rocks to the northeast with more conductive alluvial fill to the southwest. The higher RMS fit along TLVA (RMS = 5.4) was the result of one particularly noisy station, sounding #23 (Figure 24), which we chose to keep, because the model was robust and remained essentially unchanged whether or not this station was included.

Acknowledgments

This study was performed in cooperation with the Southern Nevada Water Authority whose support is greatly appreciated. We are grateful to the many people that helped us in the field, including Bill Van Stone, Carter Roberts, Casey Collins, Eric Dano, Ester Falgás Parra, Frank Baird, Harvey Eastman, Jason Mace, Keith Pari, Kevin Graves, Melissa Cansdale, Paul Jahn, Ray Schuth, Rhonda Olsen, and Tobyn VanVeghten. We thank the staff of Geometrics for providing valuable and efficient field assistance, and we especially thank Gary Dixon, Jeff Johnston, and Ester Falgás Parra for contributing their expertise and advice. We also thank Dan Scheirer and Paul Bedrosian for their helpful reviews.

References Cited

Best, M.G., Christiansen, E.H., and Blank, R.H., Jr., 1989, Oligocene caldera complex and calc-alkaline tuffs and lavas of the Indian Peak volcanic field, Nevada and Utah: Geological Society of America Bulletin, 101, p. 1076-1090.

Eberhart-Phillips, D., Stanley, W.D., Rodriguez, B.D. and Lutter, W.J., 1995, Surface seismic and electrical methods to detect fluids related to faulting: Journal of Geophysical Research, 100, p. 12,919-12,936.

Geometrics, 2000, Operation Manual for Stratagem systems running IMAGEM, Ver. 2.16: Geometrics, San Jose, California.

Geosystem, 2005, A guide to using WinGLink, Ver 2.07.05: Geosystem srl, Milan, Italy.

Harrill, J.R., and Prudic, D.E., 1998, Aquifer systems in the Great Basin region of Nevada, Utah and adjacent states – summary report: U.S. Geological Survey Professional Paper, 1409A, 61p.

Keller, G.V., 1987, Rock and mineral properties, *in* Electromagnetic Methods in Applied Geophysics Theory: M.N. Nabighian, Ed., Society of Exploration Geophysicists, Tulsa, Oklahoma, v.1, p. 13-51.

Keller, G.V., 1989, Electrical properties, *in* Carmichael, R.S., Ed., Practical handbook of physical properties of rocks and minerals: CRC Press, Boca Raton, Florida, p. 359-427.

Langenheim, V.E., Grow, J., Miller, J., Davidson, J.D., and Robison, E., 1998, Thickness of Cenozoic deposits and location and geometry of the Las Vegas Valley Shear Zone, Nevada, based on gravity, seismic-reflection, and aeromagnetic data, U.S. Geological Survey Open-File Report 98-576, 32 p.

Mankinen, E.A., Roberts, C.W., McKee, E.H., Chuchel, B.A., and Morin, R.L., 2007, Geophysical data from Spring Valley to Delamar Valley, east-central Nevada: U.S. Geological Survey Open-File Report 2007-1190, 43 p.

Mankinen, E.A., Roberts, C.W., McKee, E.H., Chuchel, B.A., and Moring, B.C., 2006, Geophysical data from the Spring and Snake valleys area, Nevada and Utah: U.S. Geological Survey Open-File Report 2006-1160, 42 p.

Marti, A., Queralt, P., Jones, A.G., and Ledo, J., 2005, Improving Bahr's invariant parameters using the WAL approach, Geophysical Journal International, 163, 38-41.

McPhee, D.K., Chuchel, B.A., and Pellerin, L, 2006, Audiomagnetotelluric data from Spring, Cave, and Coyote Spring Valleys, Nevada: U.S. Geological Survey Open-File Report 2006-1164, 41 p.

Nesbitt, B.E., 1993, Electric resistivities of crustal fluids, Journal of Geophsyical Research, 98, p.4301-4310.

Palacky, G.J., 1987, Resistivity characteristics of geologic targets, *in* Electromagnetic Methods in Applied Geophysics Theory: M.N. Nabighian, Ed., Society of Exploration Geophysicists, Tulsa, Oklahoma, vol. 1, p. 53-129.

Plume, R.W., 1996, Hydrogeologic framework of the Great Basin region of Nevada, Utah and adjacent states: U.S. Geological Survey Professional Paper 1409-B, 64p.

Rodi, W., and Mackie, R. L., 2001, Nonlinear conjugate gradients algorithm for 2-D magnetotelluric inversion, Geophysics, 66, 174-187.

Scheirer, D.S., 2005, Gravity studies of Cave, Dry Lake, and Delamar Valleys, east-central

Nevada: U.S. Geological Survey Open File Report, 2005-1339, 36p.

Telford, W.M., Geldart, L.P., and Sheriff, R.E., 1991, Applied Geophysics (2nd Edition): Cambridge University Press, 790 p.

Vozoff, K., 1991, The magnetotelluric method, *in* Electromagnetic methods in applied geophysics: M.N. Nabighian, Ed., Society of Exploration Geophysicists, Tulsa, Oklahoma, vol. 2, part B, p. 641-711.

Wannamaker, P.E., Hohmann, G.W., and Ward, S.H., 1984, Magnetotelluric responses of three-dimensional bodies in layered earths: Geophysics, 49, 1517-1533.

Weaver, J.T., Agarwal, A.K., and Lilley, F.E.M, 2000, Characterization of the magnetotelluric tensor in terms of its invariants, Geophysical Journal International, 141, 321-336.

Wright, D.E., 1988, The SEG Standard for Magnetotelluric Data: presented at the Society of Exploration Geophysicists Annual Meeting, November. Available through *http://www.geophysics.dias.ie/mtnet/docs/ediformat.txt*.

Zonge, K.L. and Hughes, L.J., 1991, Controlled source audio-frequency magnetotellurics, *in* Electromagnetic methods in applied geophysics: M.N. Nabighian, Ed., Society of Exploration Geophysicists, Tulsa, Oklahoma, vol. 2, part B, p. 713-809.

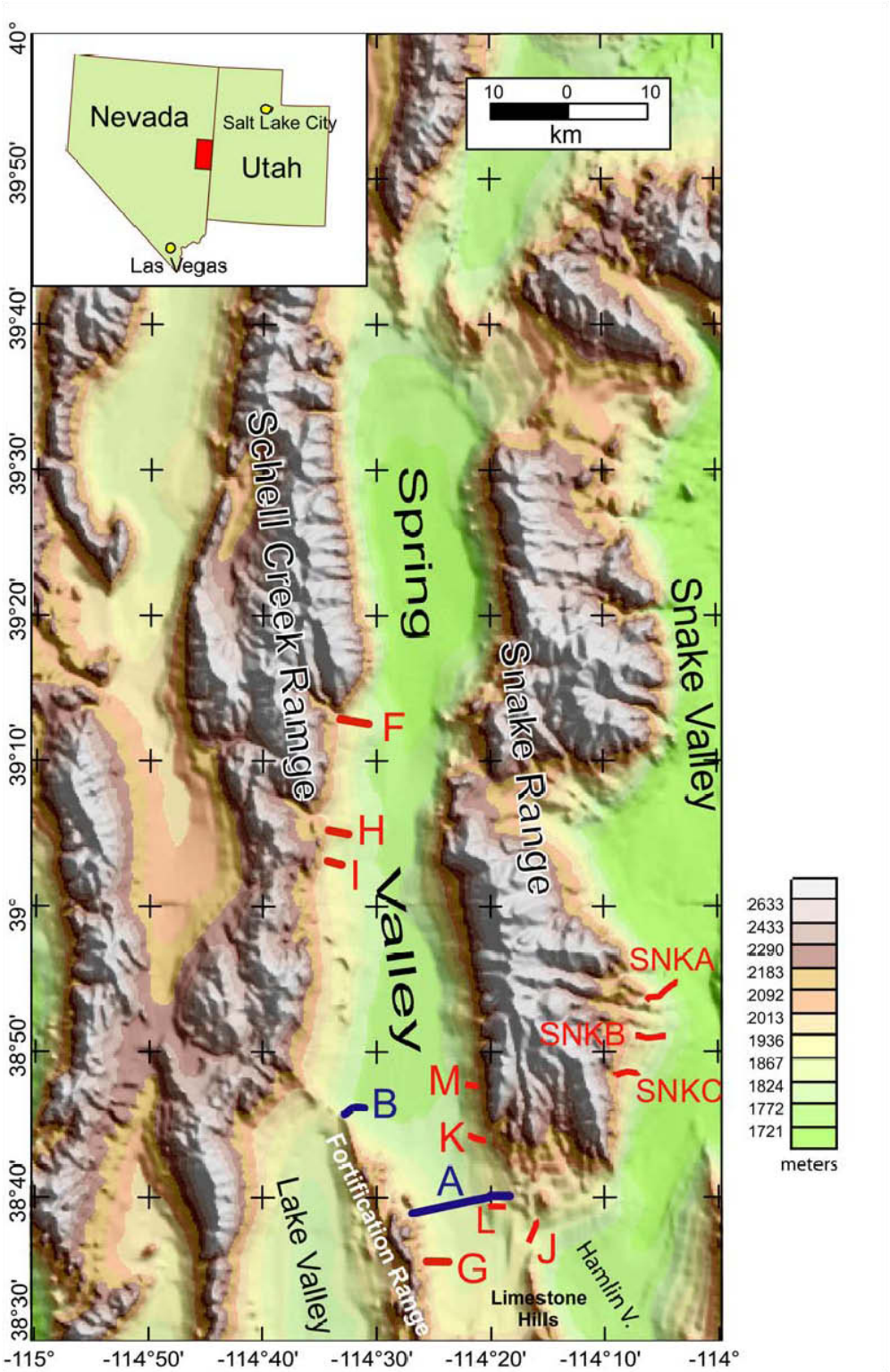

Figure 1. Topographic map of study area showing location of AMT profiles in Spring and Snake Valleys. Profiles A and B were collected in 2004 and are presented in McPhee and others (2006).

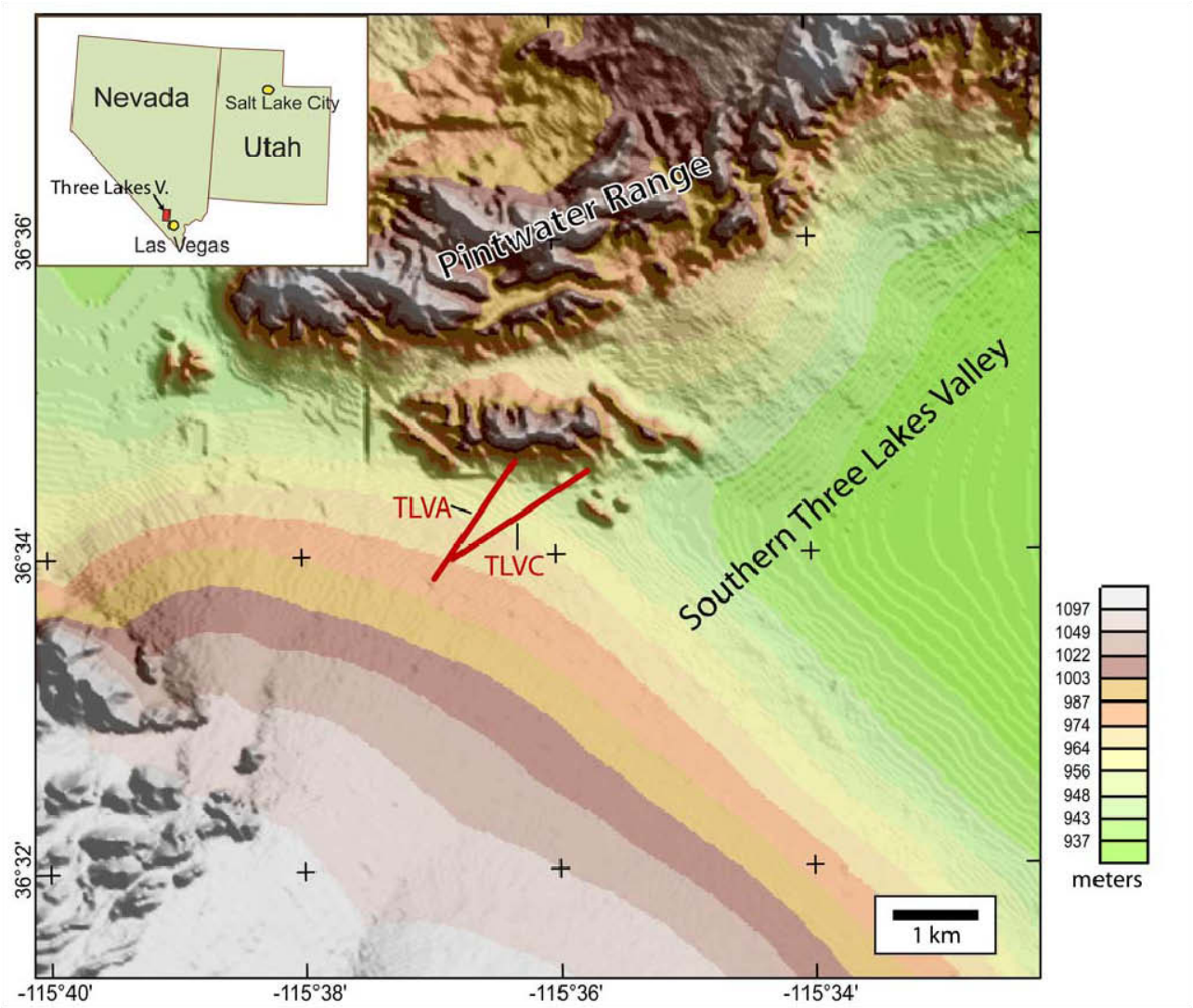

Figure 2. Topographic map of study area showing location of AMT profiles in southern Three Lakes Valley.

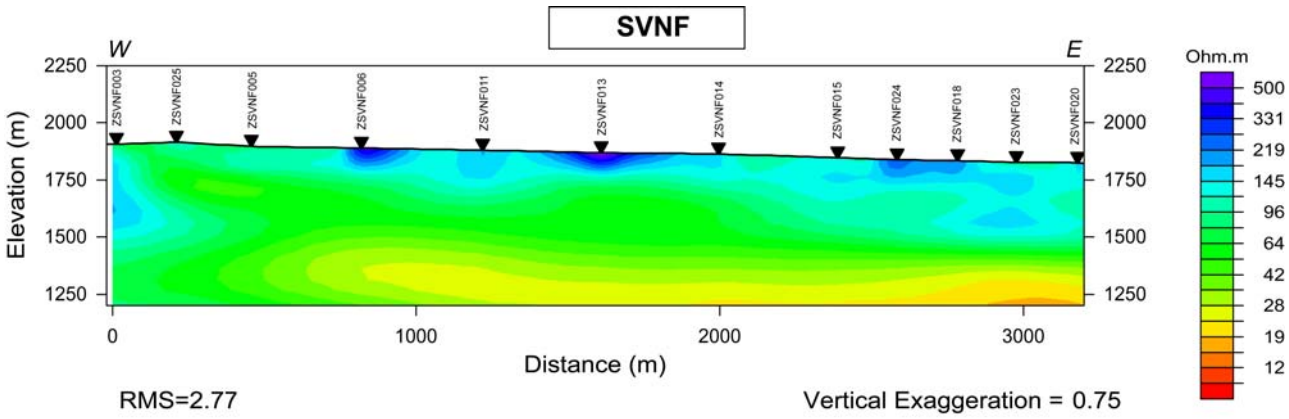

Figure 3. 2-D inverse model computed from the TM mode data along profile SVNF in Spring Valley.

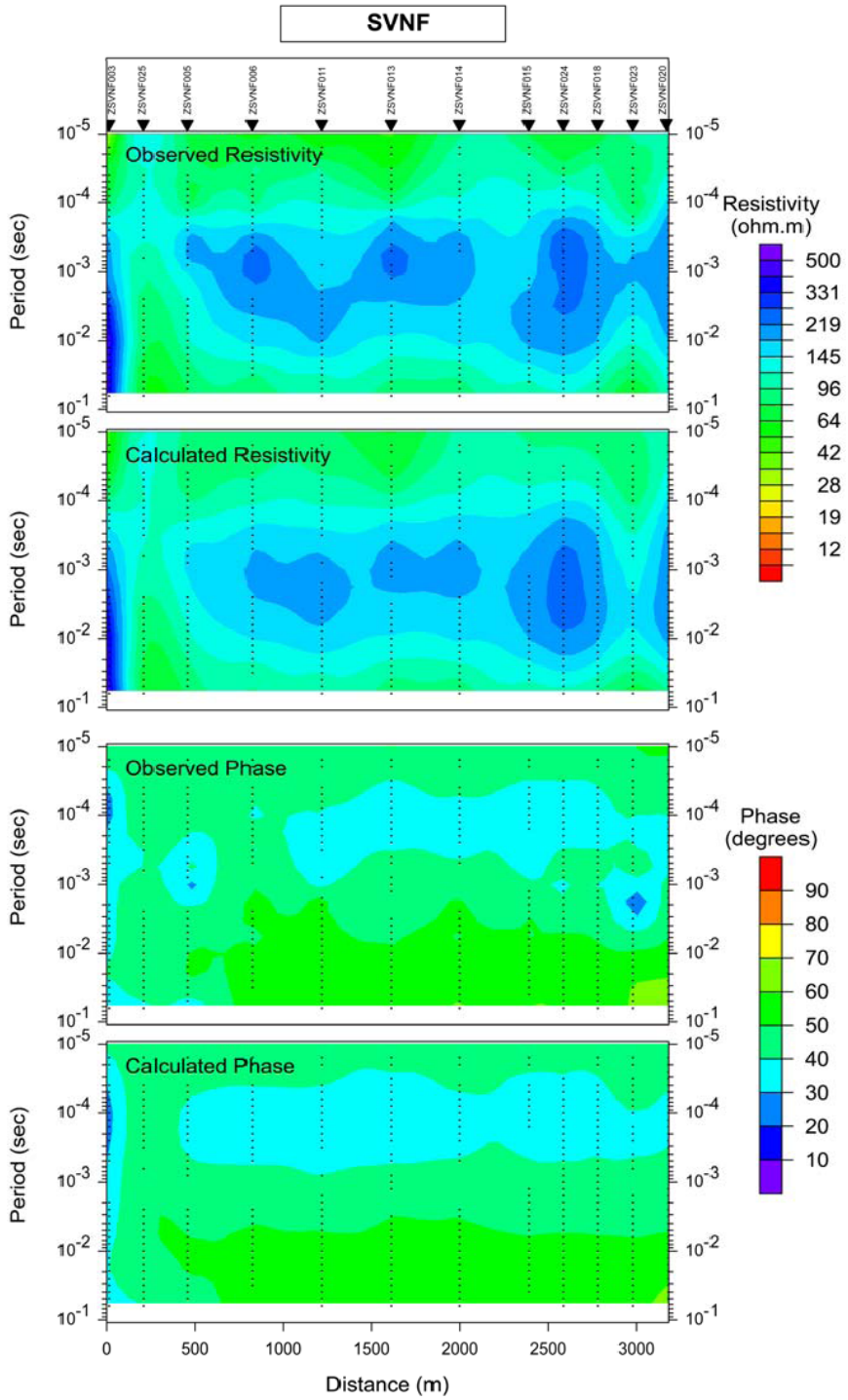

Figure 4. Pseudosections of observed data and model response for the apparent resistivity and phase along profile SVNF. Black dots show data points.

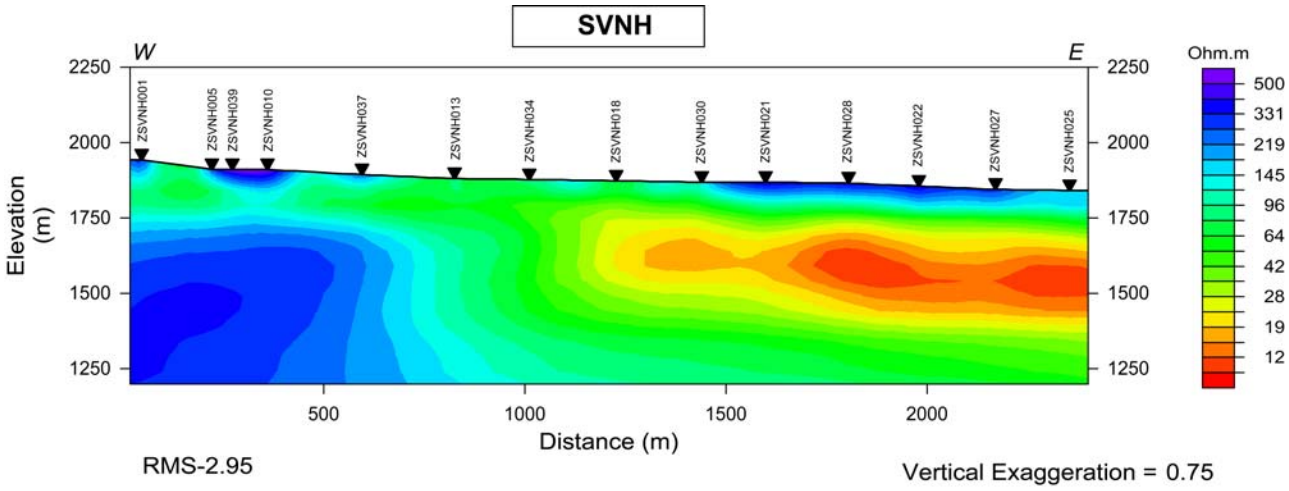

Figure 5. 2-D inverse model computed from the TM mode data along profile SVNH in Spring Valley.

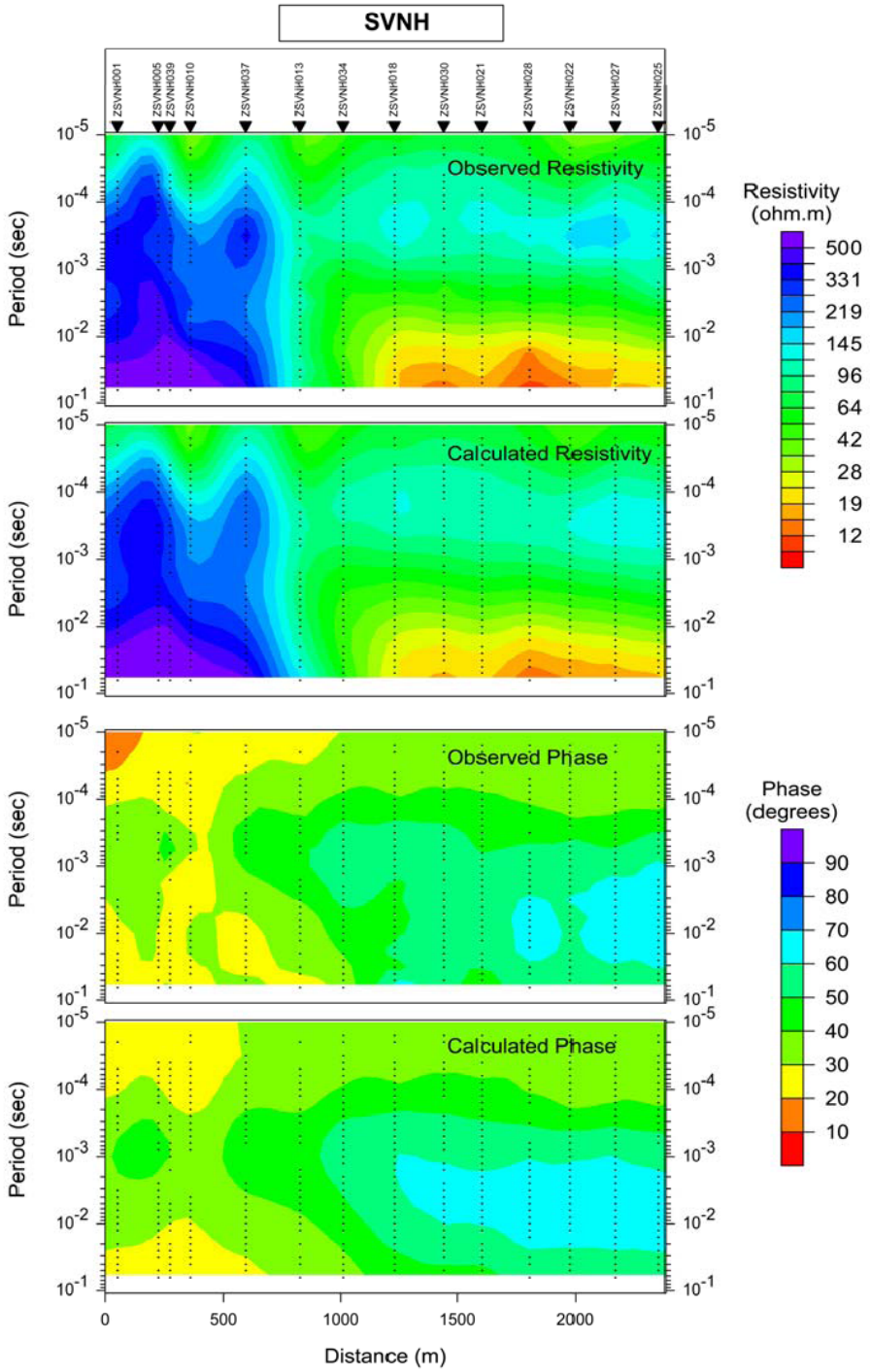

Figure 6. Pseudosections of observed data and model response for the apparent resistivity and phase along profile SVNH. Black dots show data points.

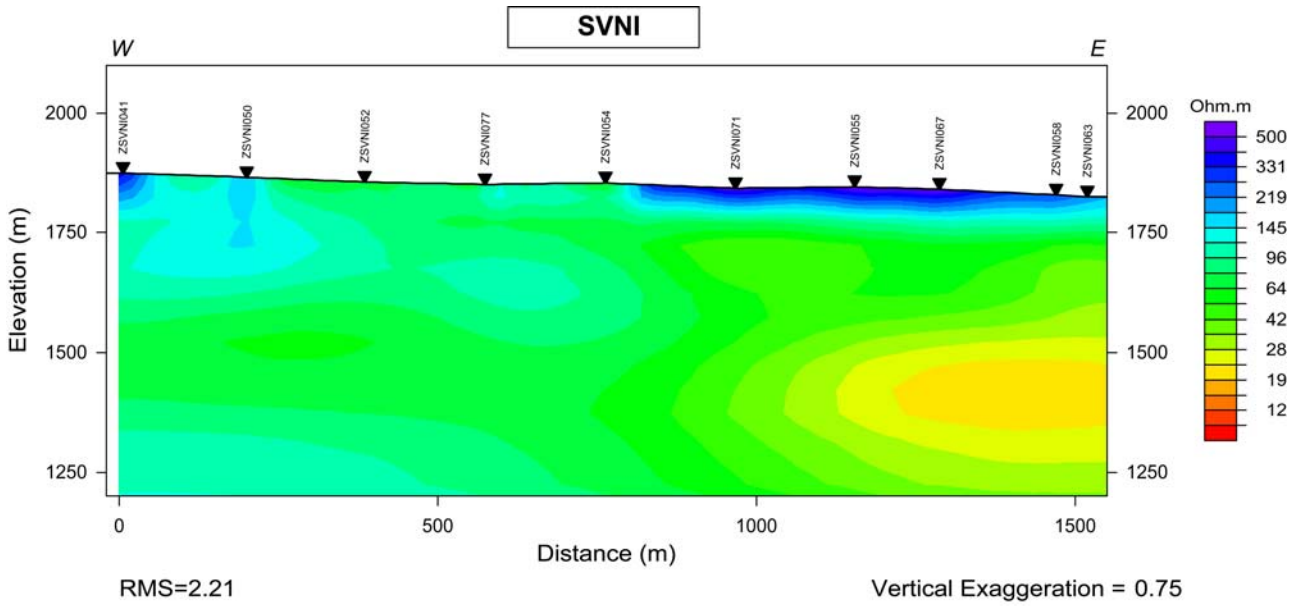

Figure 7. 2-D inverse model computed from the TM mode data along profile SVNI in Spring Valley.

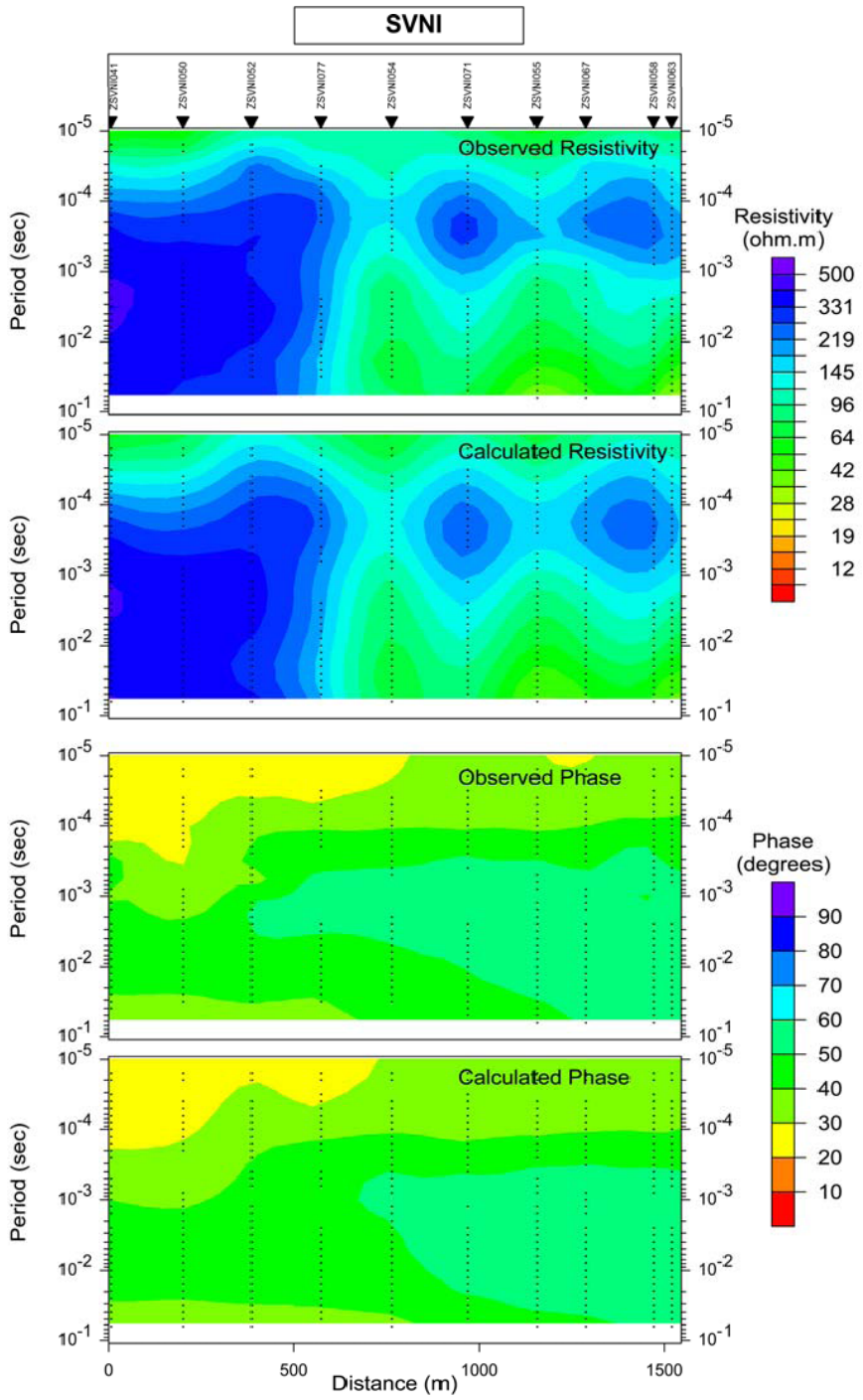

Figure 8. Pseudosections of observed data and model response for the apparent resistivity and phase along profile SVNI. Black dots show data points.

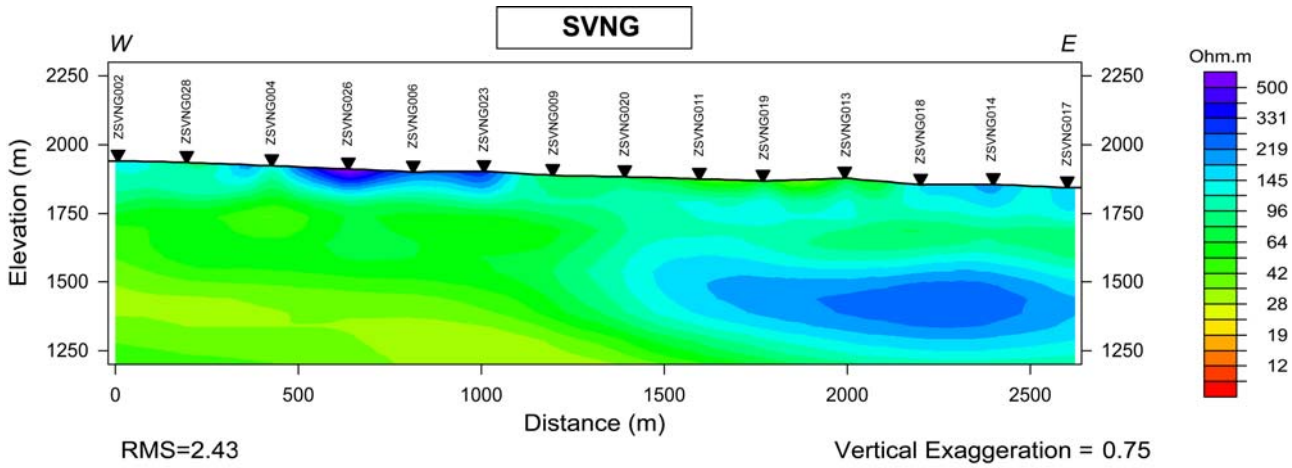

Figure 9. 2-D inverse model computed from the TM mode data along profile SVNG in Spring Valley.

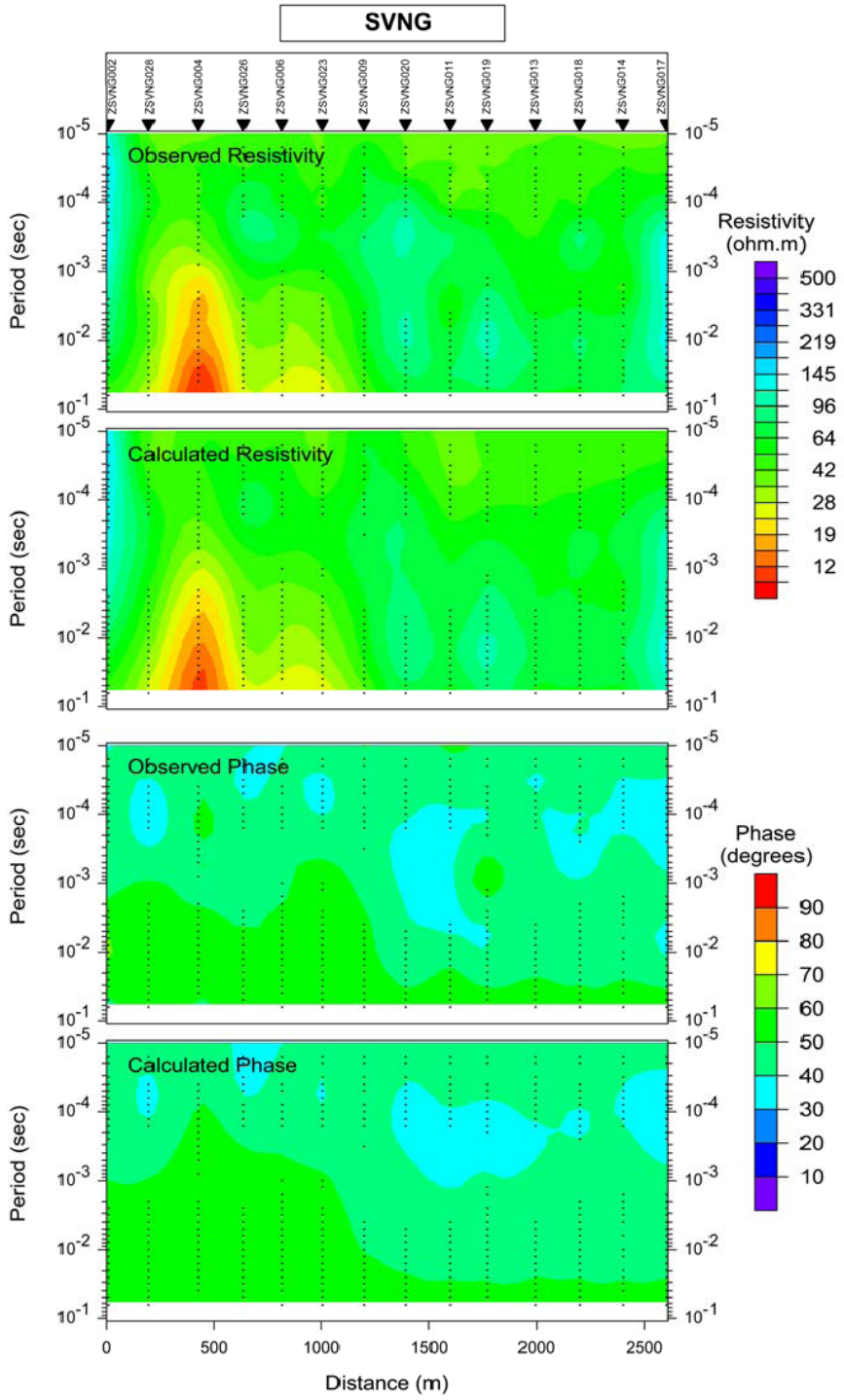

Figure 10. Pseudosections of observed data and model response for the apparent resistivity and phase along profile SVNG. Black dots show data points.

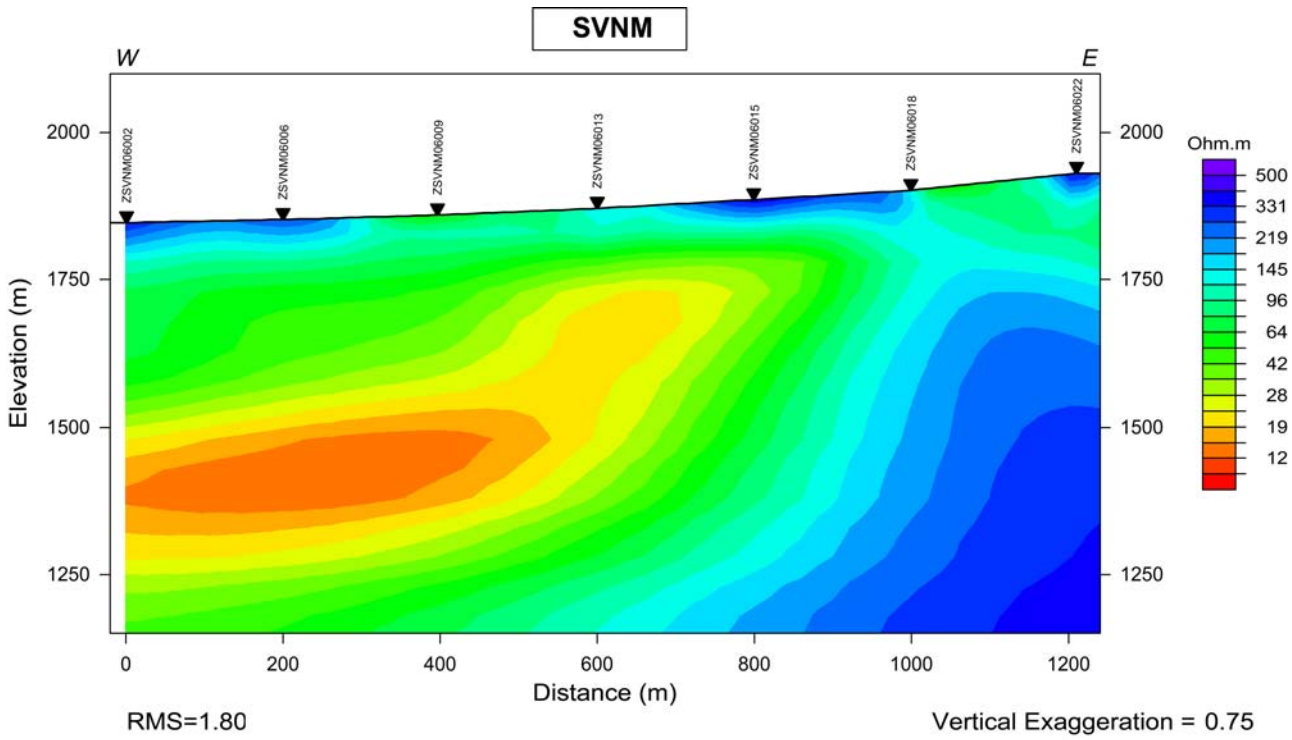

Figure 11. 2-D inverse model computed from the TM mode data along profile SVNM in Spring Valley.

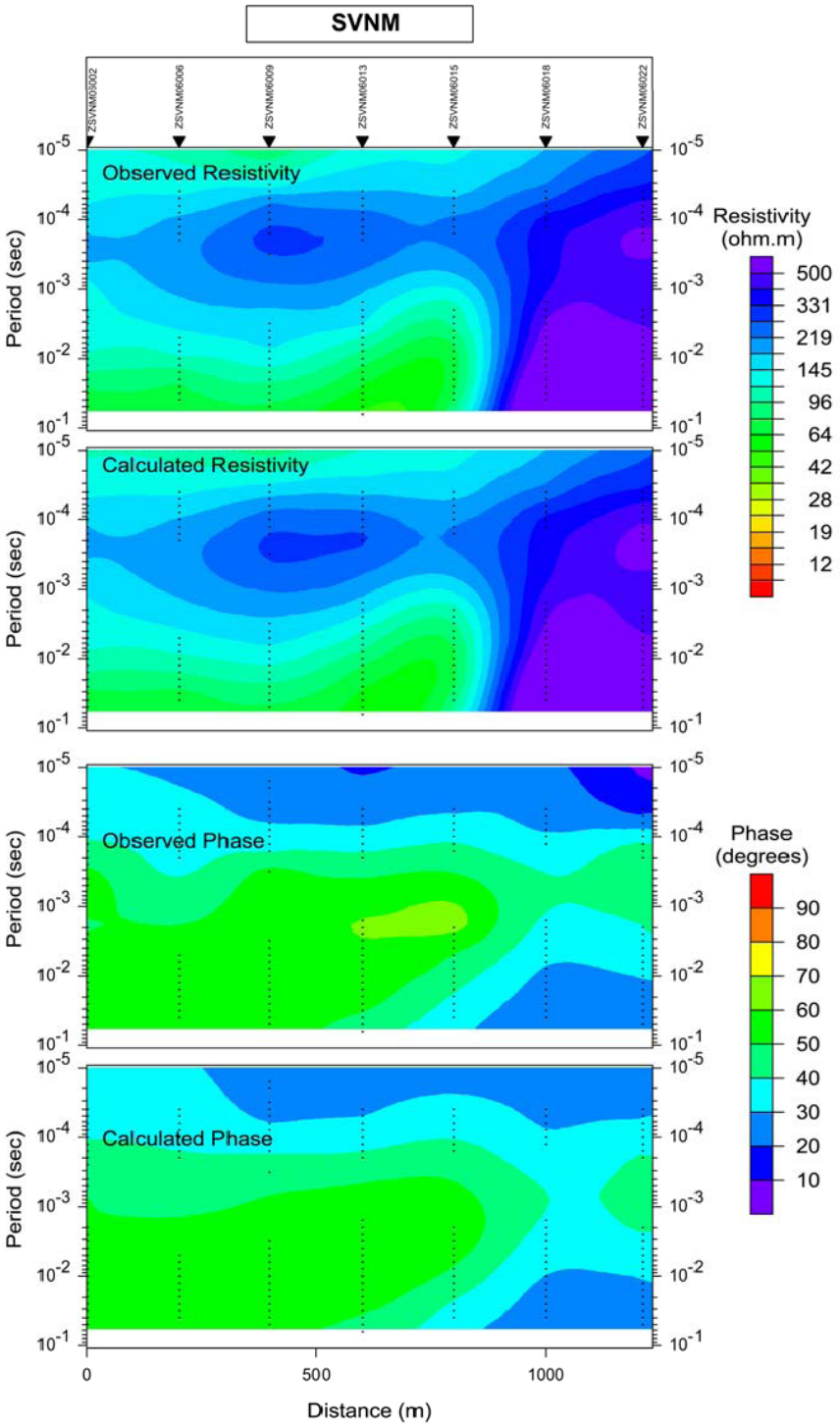

Figure 12. Pseudosections of observed data and model response for the apparent resistivity and phase along profile SVNM. Black dots show data points.

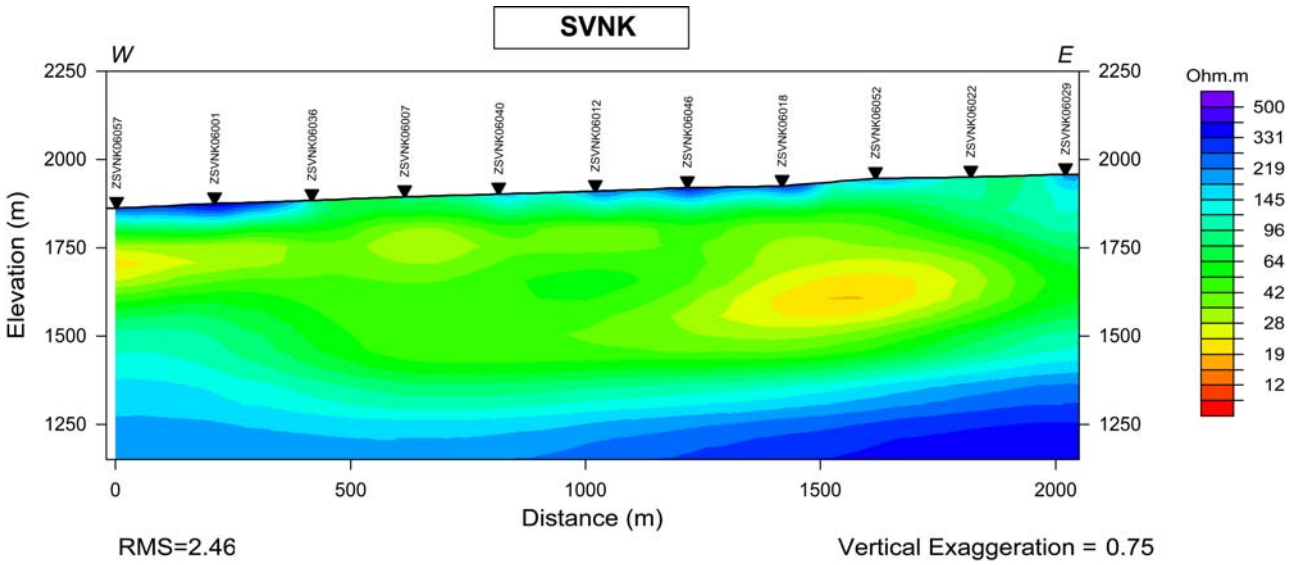

Figure 13. 2-D inverse model computed from the TM mode data along profile SVNK in Spring Valley.

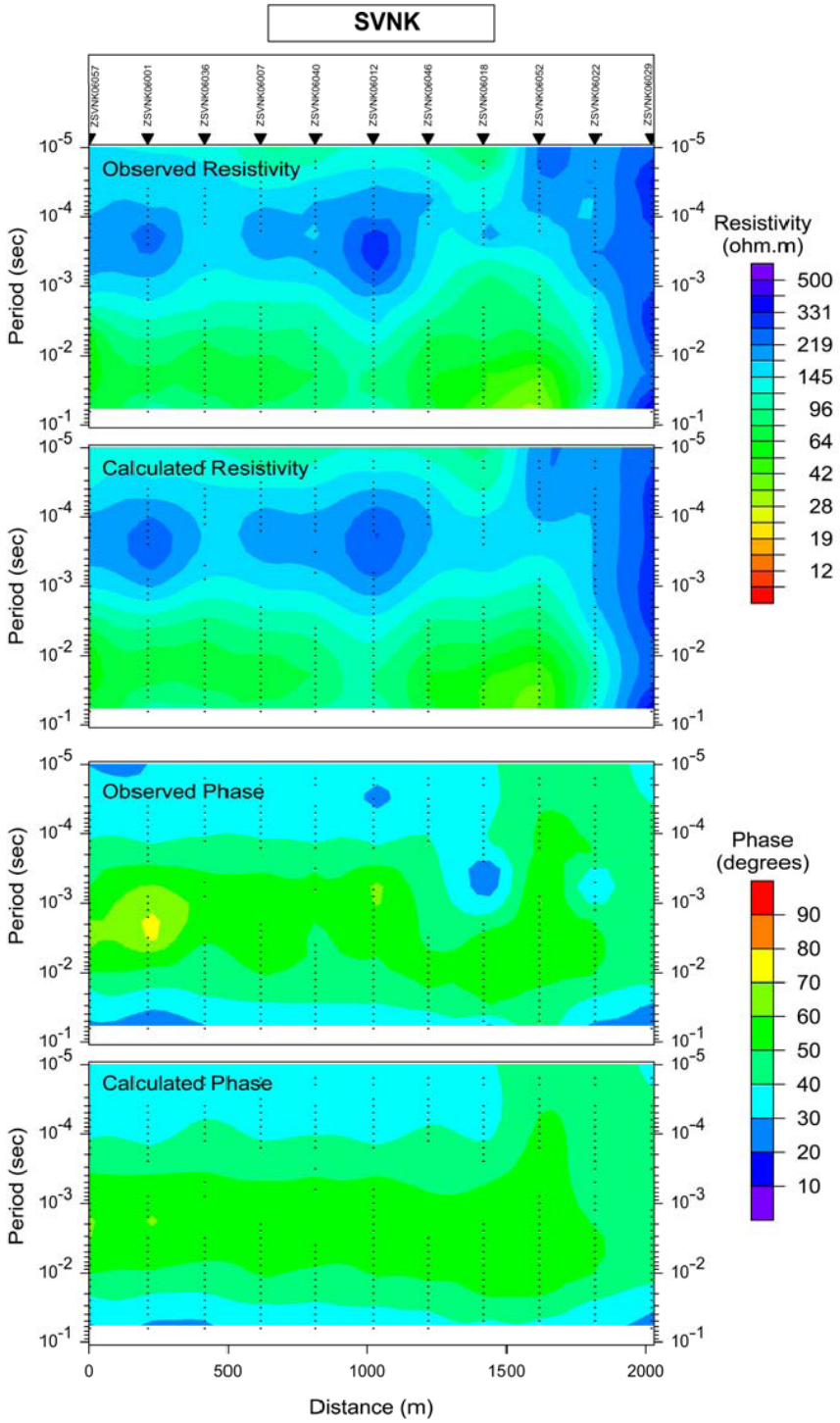

Figure 14. Pseudosections of observed data and model response for the apparent resistivity and phase along profile SVNK. Black dots show data points.

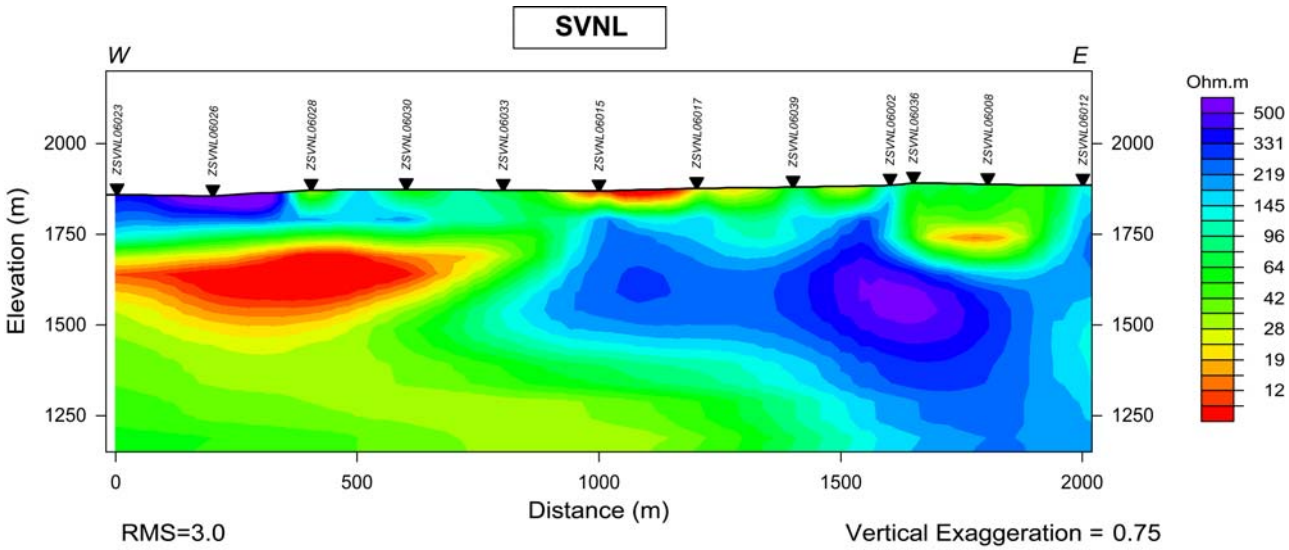

Figure 15. 2-D inverse model computed from the TM mode data along profile SVNL in Spring Valley.

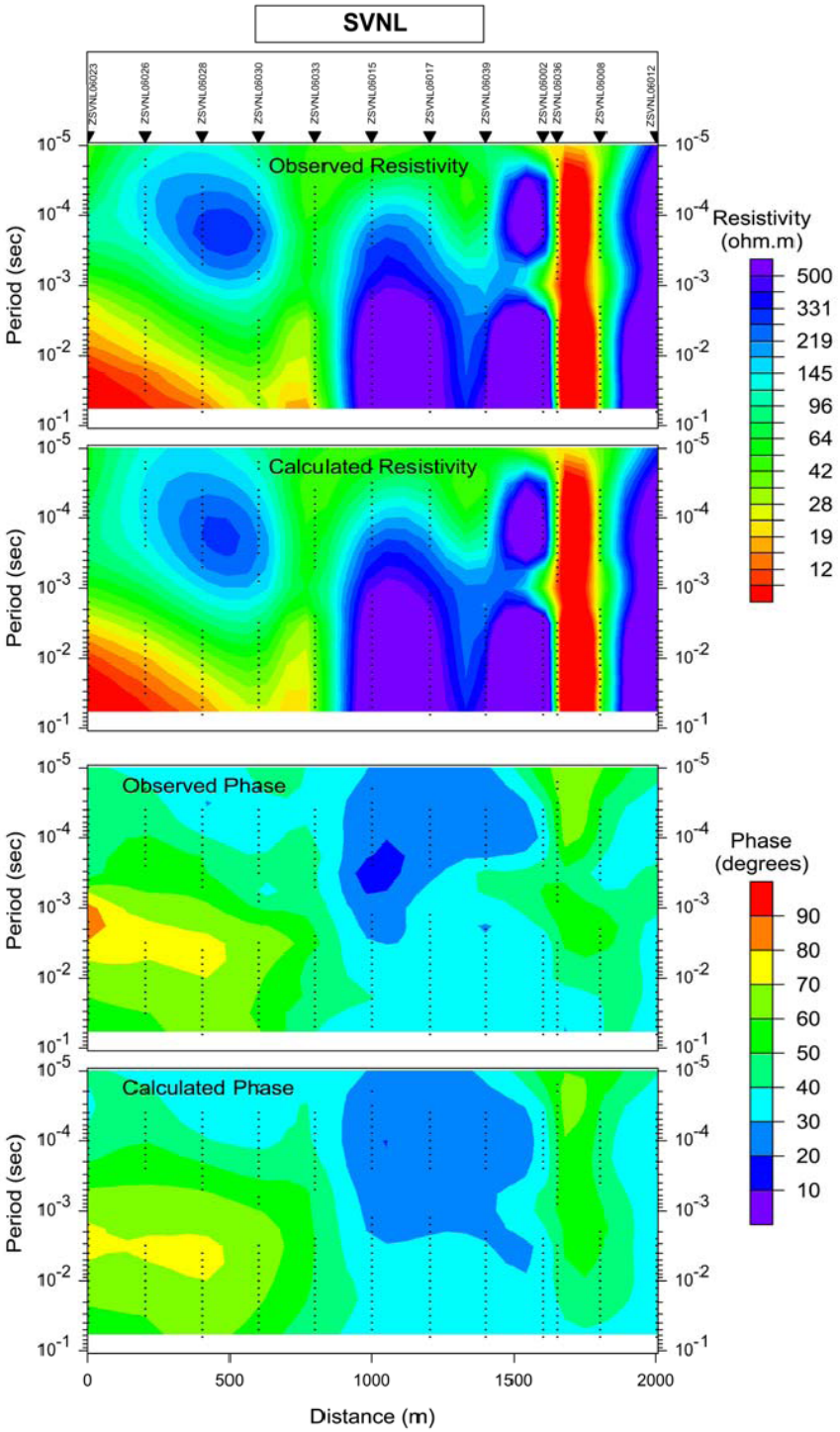

Figure 16. Pseudosections of observed data and model response for the apparent resistivity and phase along profile SVNL. Black dots show data points.

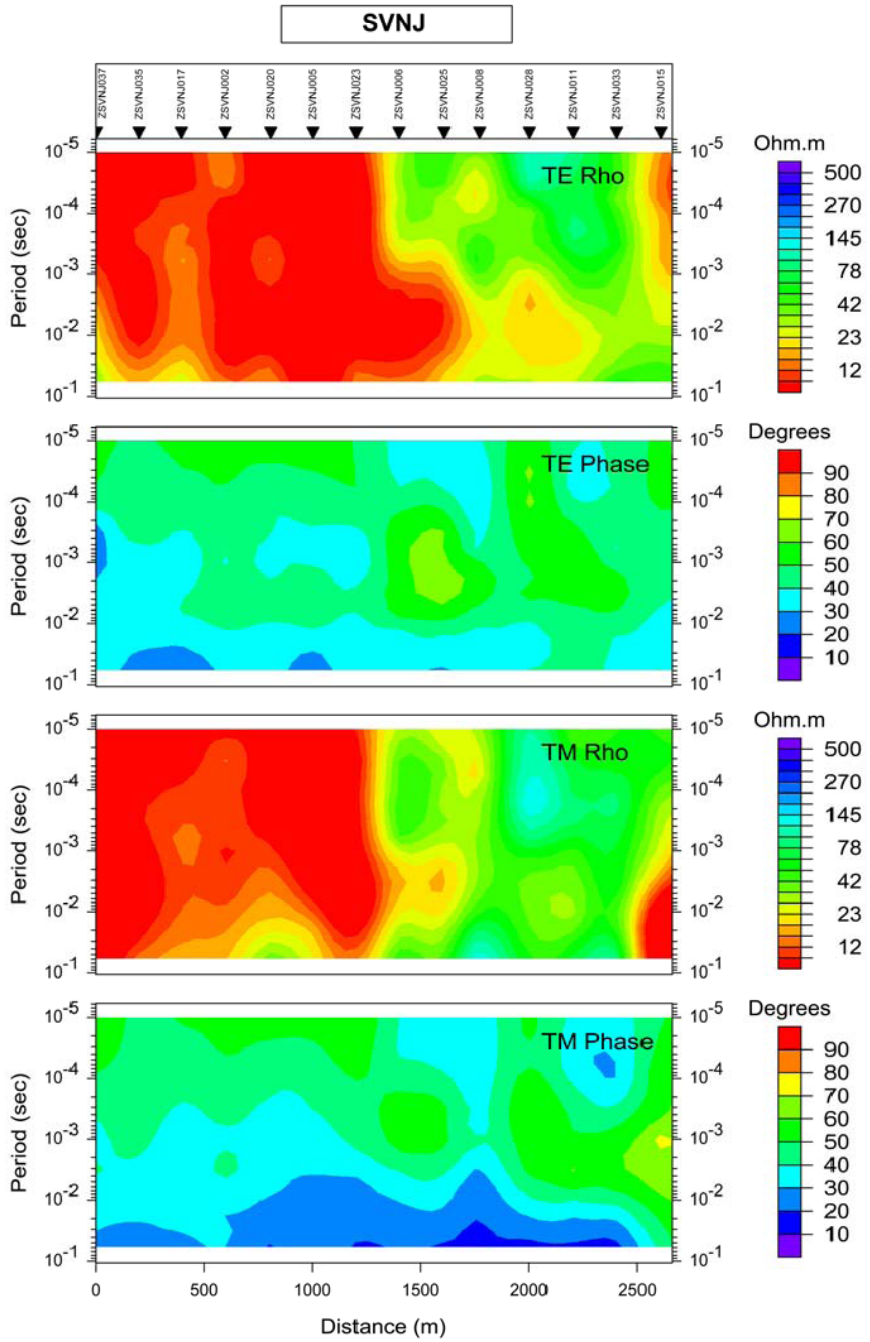

Figure 17. Pseudosections of observed data only for the TE and TM mode apparent resistivity and phase along profile SVNJ.

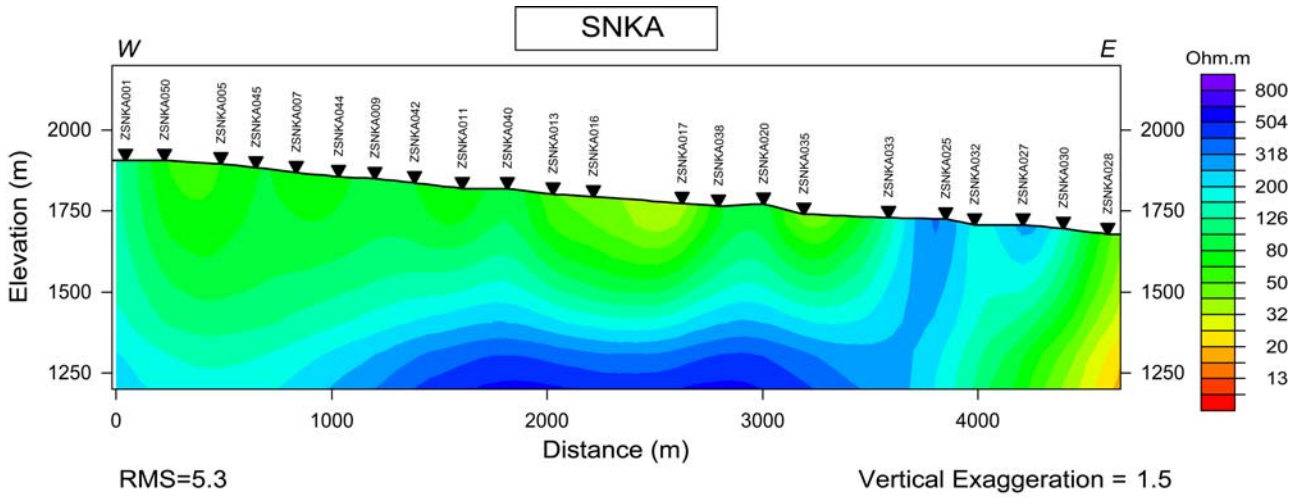

Figure 18. 2-D inverse model computed from the TM mode data along profile SNKA in Snake Valley. Note that resistivity scale is different from that used in Spring Valley models.

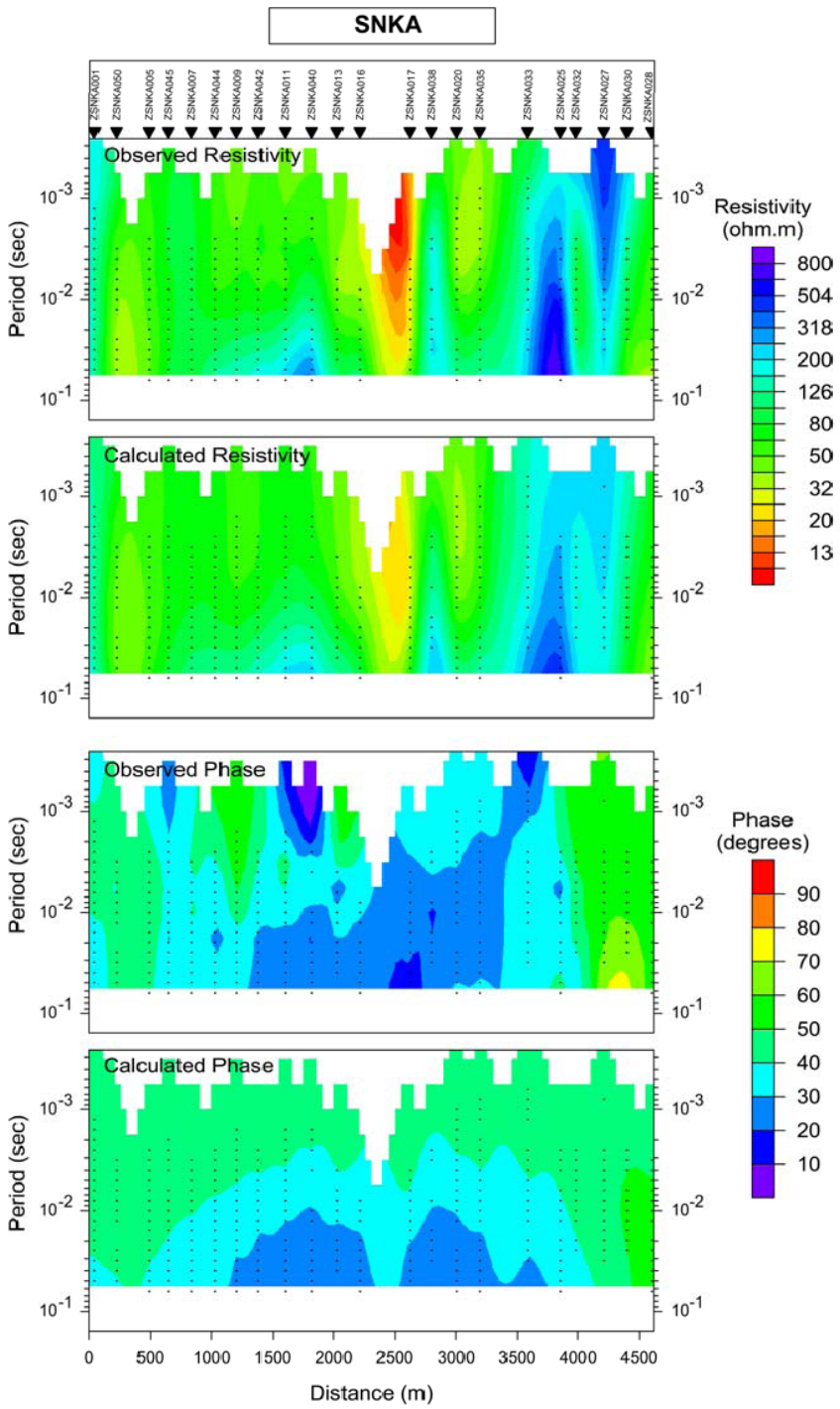

Figure 19. Pseudosections of observed data and model response for the apparent resistivity and phase along profile SNKA. Black dots show data points.

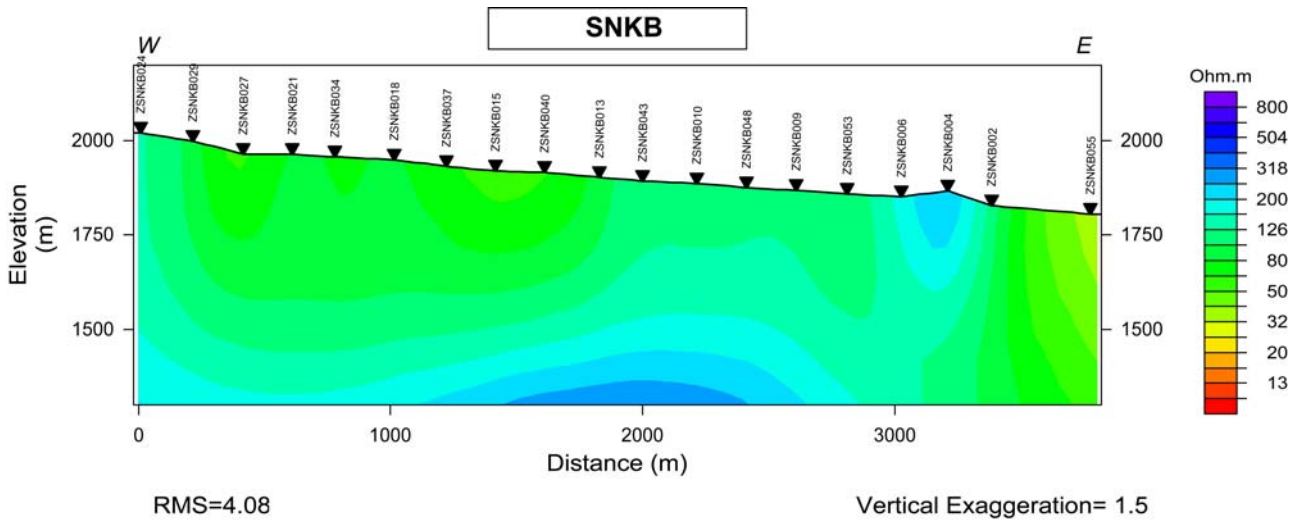

Figure 20. 2-D inverse model computed from the TM mode data along profile SNKB in Snake Valley.

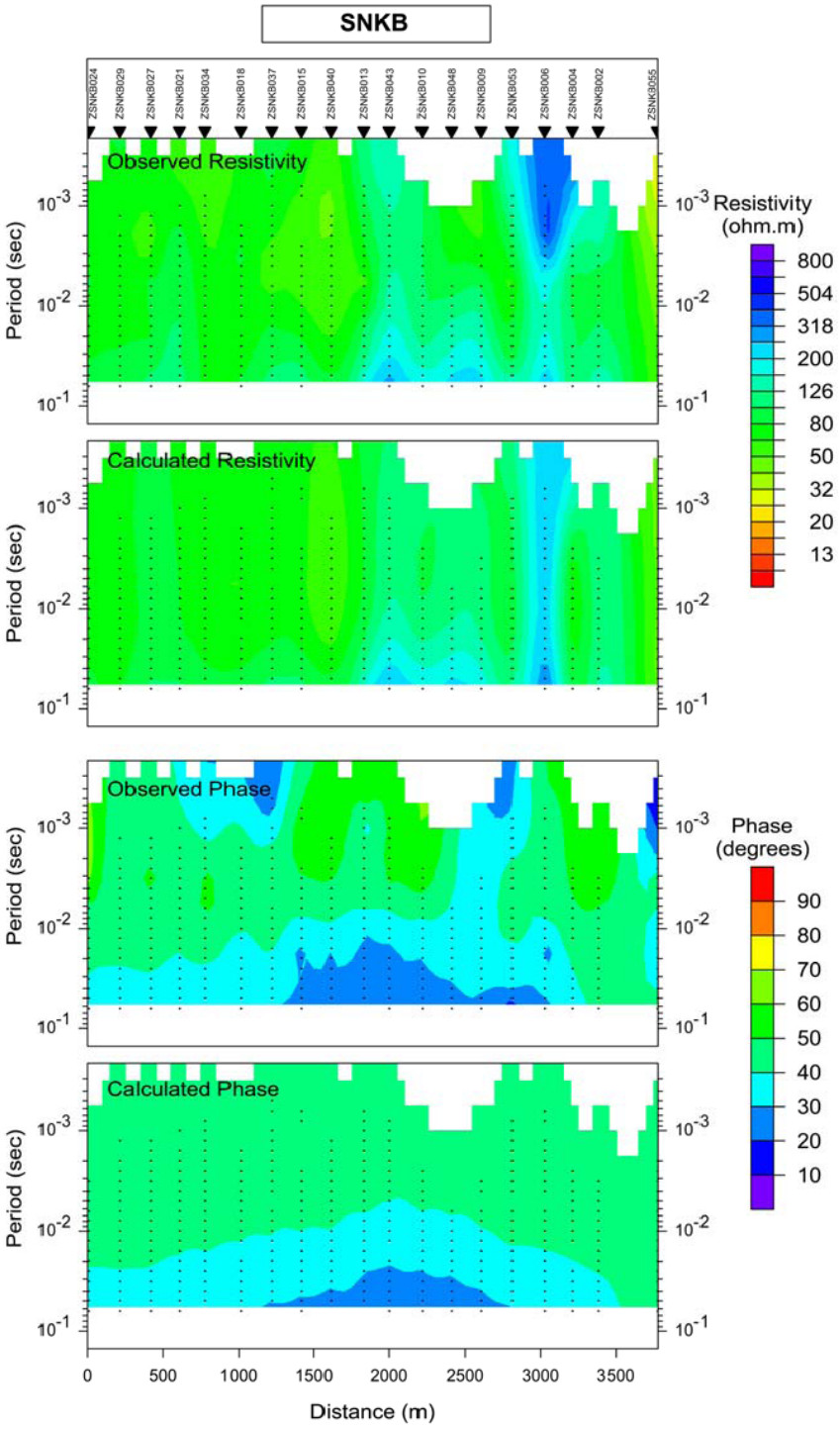

Figure 21. Pseudosections of observed data and model response for the apparent resistivity and phase along profile SNKB. Black dots show data points.

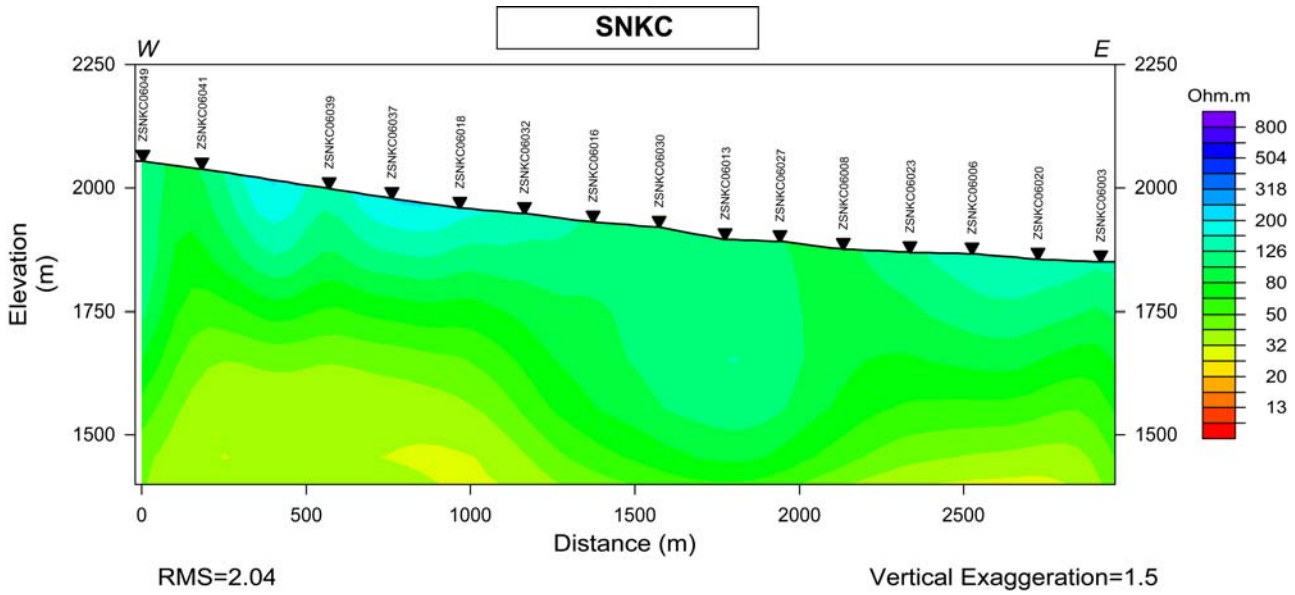

Figure 22. 2-D inverse model computed from the TM mode data along profile SNKC in Snake Valley.

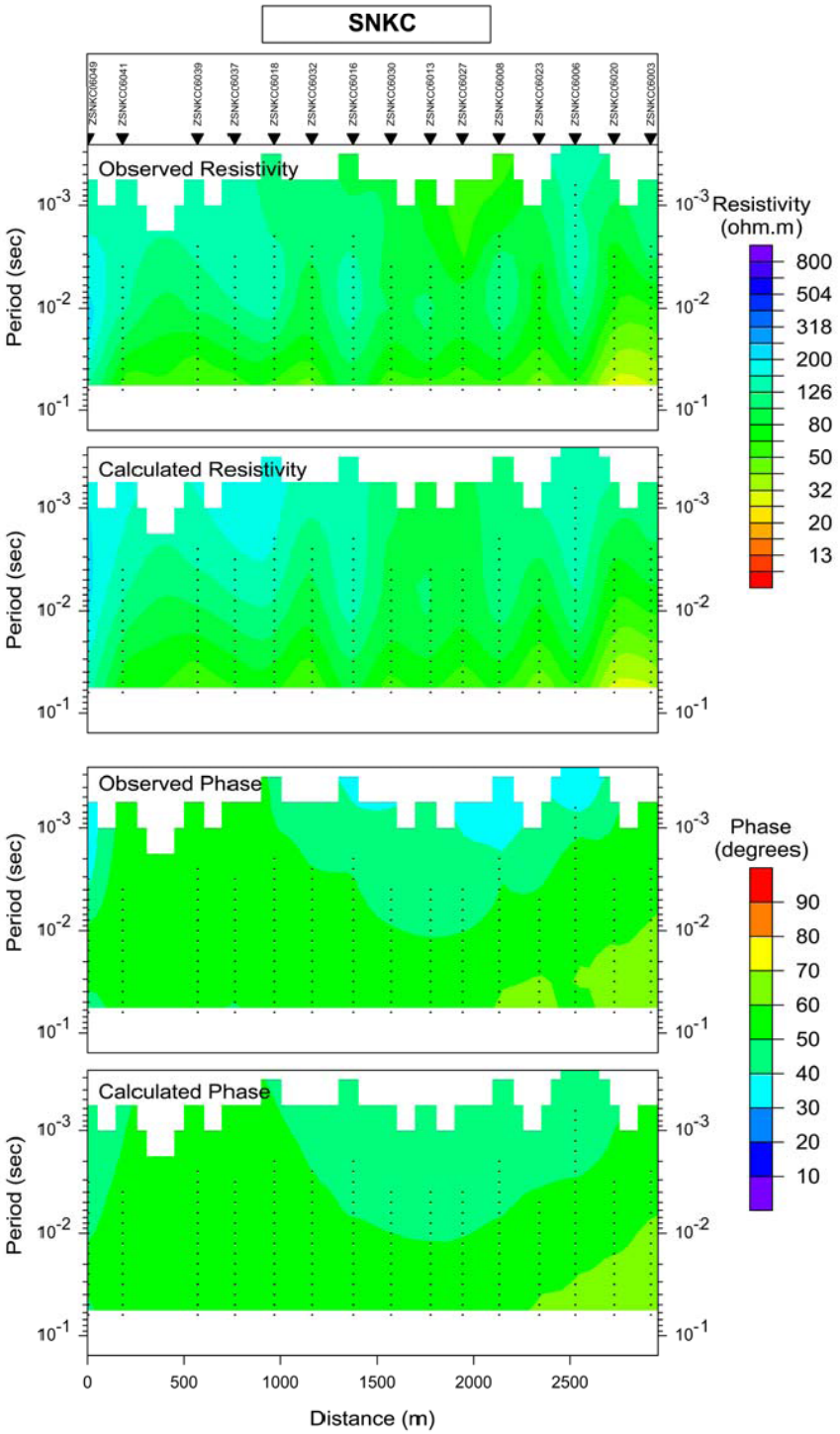

Figure 23. Pseudosections of observed data and model response for the apparent resistivity and phase along profile SNKC. Black dots show data points.

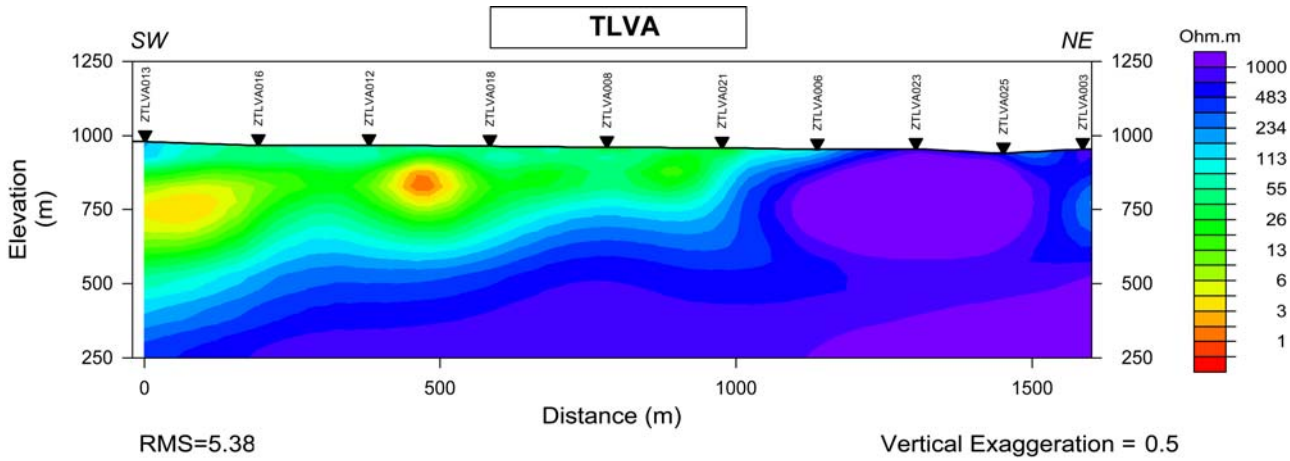

Figure 24. 2-D inverse model computed from the TE+TM mode data along profile TLVA in Three Lakes Valley. Note that resistivity scale is different from that used in Spring and Snake Valley models.

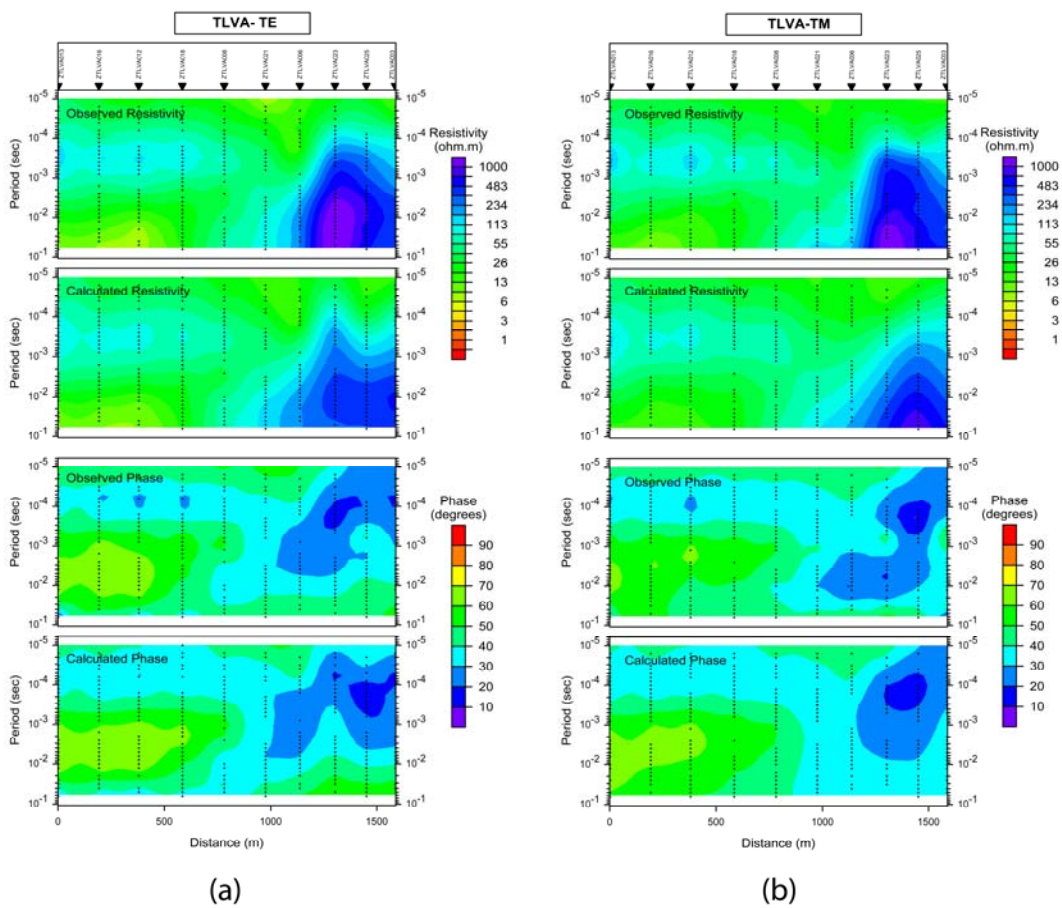

Figure 25. Pseudosections of observed data and model response for the apparent resistivity and phase along profile TLVA for both the TE (a) and TM (b) modes. Black dots show data points.

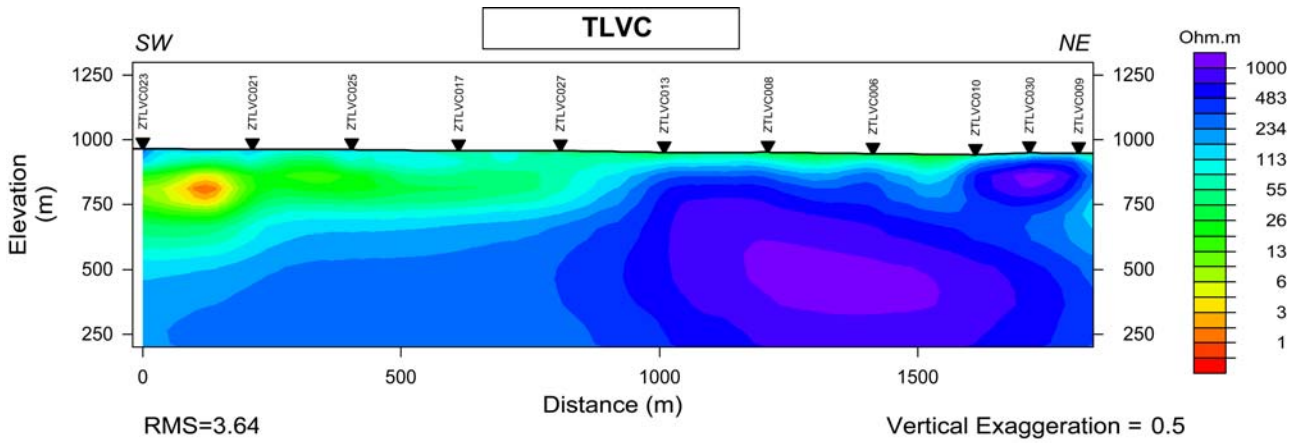

Figure 26. 2-D inverse model computed from the TE+TM mode data along profile TLVC in Three Lakes Valley.

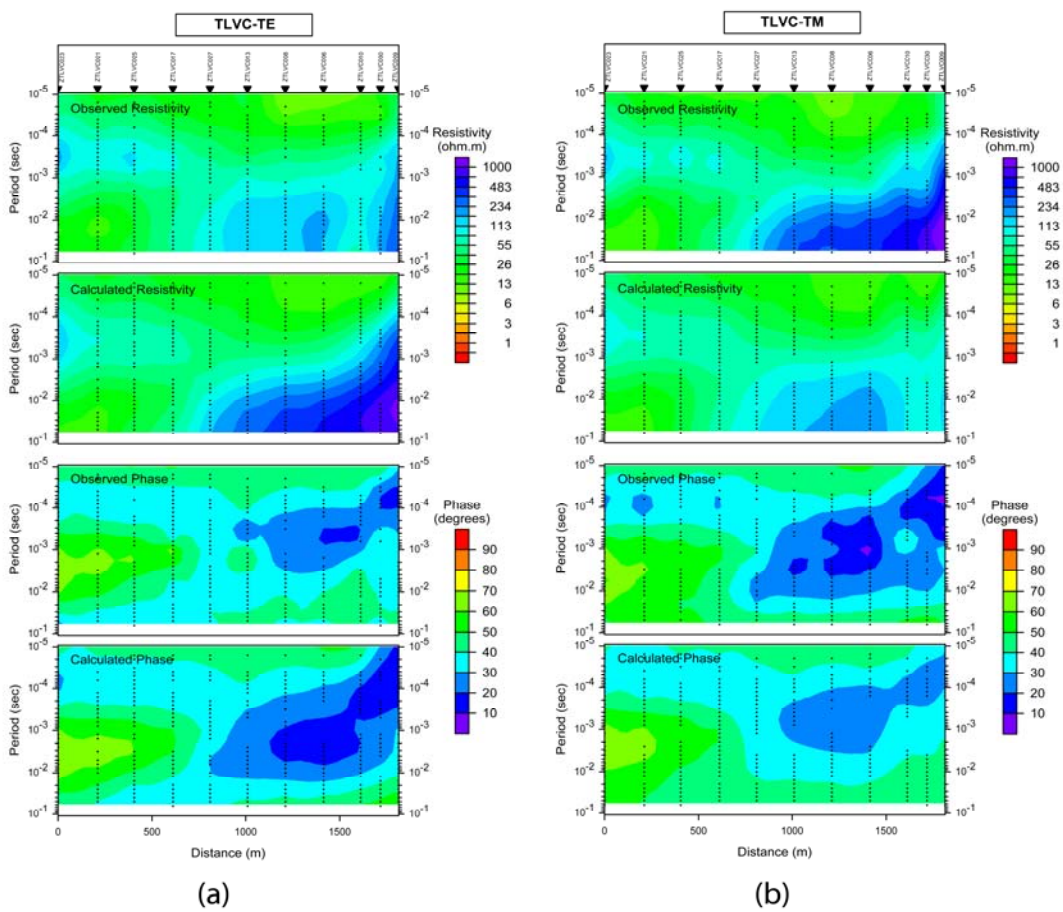

Figure 27. Pseudosections of observed data and model response for the apparent resistivity and phase along profile TLVC for both the TE (a) and TM (b) modes. Black dots show data points.

Table 1. Description of AMT profiles.

[Profile azimuth in degrees relative to magnetic North]

Profile Name	Length (km)	Profile Azimuth	Station Spacing (m)	Number of Stations	Comments
SVNF	3.25	100°	200-400	12	Western, central Spring V., near Cleve Creek
SVNH	2.4	100°	200	14	Western, central Spring V., near Cooper Creek
SVNI	1.66	104°	200	10	Western, central Spring V.
SVNG	2.6	87°	200	14	Southwestern Spring V., from margin of Fortification Range to road to Atlanta
SVNM	1.2	105°	200	7	Southeastern Spring V., near Silver Bell Mine
SVNK	2.0	105°	200	11	Southeastern Spring V., near Murphy Wash
SVNL	2.0	90°	200	12	Southeastern Spring V.
SVNJ	2.6	18°	200	14	Southeastern Spring V., pass between the Snake Range and the Limestone Hills near The Troughs
SNKA	4.6	57°	200-400	22	Southwestern Snake V.
SNKB	3.6	90°	200-400	19	Southwestern Snake V., road along Lexington Creek
SNKC	3.0	77°	200-400	15	Southwestern Snake V.
TLVA	1.6	235°	100-200	10	Southwestern Three Lakes V.
TLVC	1.8	215°	100-200	11	Southwestern Three Lakes V.

Table 2. Sounding numbers, locations, elevations and azimuths of stations along AMT profiles.

[Numbers in station name refer to distance along profile in meters (Note that not all of the profiles begin at 0000 m). Sounding is preferred sounding used in 2-D model. Horizontal locations are referenced to NAD 27, and Universal Transverse Mercator (zone 11N) units are in meters. Horizontal locations are accurate to approximately 3 m (10 ft) Station elevations are given in meters and feet and are accurate to approximately 7 m (23 ft). X azimuth refers to the orientation relative to magnetic North of the positive x-component.]

Station	Sounding	Easting (m)	Northing (m)	Elevation (ft)	Elevation (m)	X azimuth
SVNF						
SVNF0000	003	711972	4343121	6253	1906	90
SVNF0200	025	712169	4343097	6286	1916	90
SVNF0450	005	712423	4343105	6224	1897	90
SVNF0850	006	712749	4342885	6198	1889	90
SVNF1250	011	713124	4342729	6168	1880	90
SVNF1650	013	713523	4342730	6132	1869	90
SVNF2050	014	713915	4342719	6115	1864	90
SVNF2450	015	714300	4342642	6060	1847	90
SVNF2650	024	714491	4342603	6030	1838	90
SVNF2850	018	714686	4342559	6017	1834	90
SVNF3050	023	714878	4342530	5994	1827	90
SVNF3250	020	715075	4342483	5988	1825	90
SVNH						
SVNH0000	001	710719	4328688	6378	1944	90
SVNH0200	005	710906	4328737	6270	1911	90
SVNH0250	039	710964	4328771	6306	1922	90
SVNH0400	010	711064	4328830	6270	1911	90
SVNH0600	037	711305	4328837	6214	1894	90
SVNH0800	013	711516	4328721	6171	1881	90
SVNH1000	034	711694	4328662	6161	1878	90
SVNH1200	018	711912	4328653	6148	1874	90
SVNH1400	030	712136	4328695	6132	1869	90
SVNH1600	021	712302	4328714	6132	1869	90
SVNH1800	028	712486	4328582	6122	1866	90
SVNH2000	022	712643	4328471	6089	1856	90
SVNH2200	027	712810	4328327	6053	1845	90
SVNH2400	025	712982	4328246	6043	1842	90
SVNI						
SVNI0000	041	710826	4324916	6152	1875	90
SVNI0200	050	711019	4324890	6122	1866	90
SVNI0400	052	711185	4324788	6089	1856	90

SVNI0600	077	711356	4324690	6073	1851	90
SVNI0800	054	711530	4324601	6083	1854	90
SVNI1000	071	711721	4324522	6047	1843	90
SVNI1200	055	711894	4324443	6056	1846	90
SVNI1400	067	712052	4324532	6040	1841	90
SVNI1600	058	712249	4324573	6001	1829	90
SVNI1660	063	712306	4324600	5988	1825	90
SVNG						
SVNG0000	002	724323	4274128	6368	1941	90
SVNG0200	028	724511	4274134	6348	1935	90
SVNG0400	004	724742	4274146	6309	1923	90
SVNG0600	026	724953	4274138	6270	1911	90
SVNG0800	006	725129	4274168	6237	1901	90
SVNG1000	023	725321	4274177	6243	1903	90
SVNG1200	009	725510	4274188	6194	1888	90
SVNG1400	020	725707	4274195	6178	1883	90
SVNG1600	011	725910	4274199	6152	1875	90
SVNG1800	019	726084	4274210	6129	1868	90
SVNG2000	013	726307	4274214	6161	1878	90
SVNG2200	018	726515	4274220	6083	1854	90
SVNG2400	014	726712	4274238	6086	1855	90
SVNG2600	017	726915	4274248	6047	1843	90
SVNM						
SVNM0400	002	728616	4297449	6060	1847	80
SVNM0600	006	728800	4297366	6077	1852	80
SVNM0800	009	728982	4297287	6102	1860	80
SVNM1000	013	729173	4297215	6139	1871	80
SVNM1200	015	729368	4297173	6188	1886	80
SVNM1400	018	729564	4297131	6240	1902	80
SVNM1600	022	729801	4297200	6335	1931	80
SVNK						
SVNK0200	057	729177	4290814	6109	1862	60
SVNK0400	001	729371	4290736	6152	1875	60
SVNK0600	036	729573	4290690	6180	1884	60
SVNK0800	007	729764	4290639	6215	1894	60
SVNK1000	040	729955	4290578	6240	1902	60
SVNK1200	012	730155	4290529	6267	1910	60
SVNK1400	046	730340	4290463	6299	1920	60
SVNK1600	018	730532	4290402	6315	1925	60
SVNK1800	052	730724	4290351	6385	1946	60
SVNK2000	022	730925	4290316	6398	1950	60
SVNK2200	029	731129	4290296	6424	1958	60
SVNL						
SVNL0400	023	731793	4281872	6100	1859	80

SVNL0600	026	731992	4281883	6087	1855	80
SVNL0800	028	732194	4281895	6141	1872	80
SVNL1000	030	732391	4281896	6148	1874	80
SVNL1200	033	732592	4281903	6141	1872	80
SVNL1400	015	732790	4281903	6133	1869	80
SVNL1600	017	732992	4281913	6158	1877	80
SVNL1800	039	733192	4281917	6167	1880	80
SVNL2000	002	733392	4281927	6184	1885	80
SVNL2050	036	733441	4281922	6207	1892	80
SVNL2200	008	733594	4281938	6192	1887	80
SVNL2400	012	733791	4281939	6184	1885	80
SVNJ						
SVNJ0200	037	737155	4277622	6029	1838	60
SVNJ0400	035	737229	4277808	6017	1834	60
SVNJ0600	017	737299	4277987	6006	1831	60
SVNJ0800	002	737368	4278180	5977	1822	60
SVNJ1000	020	737451	4278371	5987	1825	60
SVNJ1200	005	737521	4278554	5994	1827	60
SVNJ1400	023	737596	4278739	6012	1832	60
SVNJ1600	006	737664	4278924	6021	1835	60
SVNJ1800	025	737677	4279142	6065	1849	60
SVNJ2000	008	737799	4279272	6057	1846	60
SVNJ2200	028	737901	4279480	6081	1853	60
SVNJ2400	011	737976	4279666	6120	1865	60
SVNJ2600	033	737946	4279889	6122	1866	60
SVNJ2800	015	737890	4280124	6164	1879	60
SNKA						
SNKA0000	001	751105	4308783	6259	1908	90
SNKA0200	050	751246	4308897	6255	1907	135
SNKA0440	005	751494	4308996	6221	1896	90
SNKA0600	045	751648	4309057	6184	1885	135
SNKA0800	007	751855	4309077	6132	1869	135
SNKA1000	044	752066	4309114	6090	1856	135
SNKA1200	009	752260	4309122	6072	1851	135
SNKA1400	042	752448	4309167	6028	1837	135
SNKA1600	011	752652	4309259	5973	1821	135
SNKA1800	040	752828	4309377	5969	1819	135
SNKA2000	013	752999	4309501	5912	1802	135
SNKA2200	016	753142	4309624	5891	1796	135
SNKA2630	017	753401	4309983	5821	1774	135
SNKA2800	038	753553	4310061	5793	1766	135
SNKA3000	020	753709	4310207	5815	1772	135
SNKA3200	035	753857	4310320	5711	1741	135
SNKA3600	033	754180	4310545	5676	1730	135
SNKA3800	025	754405	4310689	5661	1725	135
SNKA4000	032	754505	4310779	5604	1708	135

SNKA4200	027	754680	4310925	5603	1708	90
SNKA4400	030	754828	4311041	5566	1697	135
SNKA4600	028	754997	4311154	5509	1679	135
SNKB						
SNKB0000	024	749922	4304136	6554	2021	90
SNKB0200	029	750129	4304142	6481	1999	90
SNKB0400	027	750330	4304111	6446	1965	90
SNKB0600	021	750525	4304091	6370	1965	135
SNKB0800	034	750697	4303999	6346	1957	90
SNKB1000	018	750932	4303941	6322	1950	135
SNKB1200	037	751141	4303898	6266	1932	135
SNKB1400	015	751334	4303990	6225	1920	135
SNKB1600	040	751529	4303985	6213	1916	135
SNKB1800	013	751748	4303956	6171	1903	135
SNKB2000	043	751919	4303966	6139	1893	135
SNKB2200	010	752132	4304009	6117	1886	135
SNKB2400	048	752327	4304073	6084	1876	135
SNKB2600	009	752523	4304115	6057	1868	135
SNKB2800	053	752726	4304106	6027	1859	135
SNKB3000	006	752942	4304116	6005	1852	135
SNKB3200	004	753125	4304171	6054	1867	135
SNKB3400	002	753300	4304168	5927	1828	135
SNKB3800	055	753690	4304207	5925	1806	135
SNKC						
SNKC0600	049	747492	4298975	6740	2054	20
SNKC0800	041	747652	4299078	6687	2038	45
SNKC1200	039	748007	4299258	6556	1998	35
SNKC1400	037	748187	4299325	6491	1978	45
SNKC1600	018	748383	4299395	6427	1959	55
SNKC1800	032	748578	4299422	6390	1948	90
SNKC2000	016	748774	4299501	6334	1931	90
SNKC2200	030	748976	4299516	6299	1920	90
SNKC2400	013	749180	4299528	6219	1896	90
SNKC2600	027	749373	4299443	6205	1891	90
SNKC2800	008	749587	4299372	6154	1876	90
SNKC3000	023	749787	4299409	6133	1869	90
SNKC3200	006	749966	4299474	6123	1866	90
SNKC3400	020	750161	4299517	6087	1855	90
SNKC3600	003	750363	4299499	6069	1850	90
TLVA						
TLVA0000	003	624772	4048581	3129	954	180
TLVA0150	025	624691	4048474	3083	940	225
TLVA0300	023	624608	4048352	3133	955	180
TLVA0450	006	624543	4048195	3126	953	180
TLVA0600	021	624441	4048069	3146	959	225

TLVA0800	008	624339	4047904	3149	960	225
TLVA1000	018	624248	4047726	3162	964	225
TLVA1200	012	624104	4047578	3175	968	225
TLVA1400	016	623968	4047445	3172	967	225
TLVA1600	013	623868	4047282	3211	979	225
TLVC						
TLVC0000-2	009	625600	4048481	3106	947	225
TLVC0100	030	625525	4048420	3116	950	225
TLVC0200	010	625440	4048360	3090	942	225
TLVC0400	006	625284	4048236	3103	946	225
TLVC0600	008	625111	4048130	3123	952	225
TLVC0800	013	624937	4048028	3120	951	225
TLVC1000	027	624764	4047926	3143	958	225
TLVC1200	017	624588	4047835	3139	957	225
TLVC1400	025	624413	4047723	3156	962	225
TLVC1600	021	624280	4047575	3159	963	225
TLVC1800	023	624088	4047483	3166	965	225

Appendix

A. Sounding curves.

The “Audiomagnetotelluric Data” section in this report contains an explanation for three separate plots for each station:

1. Apparent Resistivity curves with x-directed along profile such that the nominal TM mode is ExHy (red diamond) and TE is EyHx (blue square).
2. Impedance Phase curves with x-directed along profile such that the nominal TM mode is ExHy (red diamond) and TE is EyHx (blue square).
3. Multiple E-Predicted Coherencies, defined as (ExHy * Conj(ExHy)) / (Hy * Conj(Hy) * Ex * Conj(Ex)) (red diamond) and (EyHx * Conj(EyHx)) / (Hx * Conj(Hx) * Ey * Conj(Ey)) (blue square)

Sounding curves are named by profile name and distance along the profile (m).